Stimulated photon echo for angular analysis of elastic and depolarizing Yb*—noble-gas collisions

J. C. Keller and J. L. Le Gouët
Laboratoire Aimé Cotton, Centre National de la Recherche Scientifique II, Bâtiment 505, 91405 Orsay Cedex, France
(Received 2 January 1985)

Elastic and depolarizing collisions between excited ytterbium atoms ($6s\,6p\,^3P_1$ level) and noble gases (He, Ne, and Xe) are investigated using a stimulated-photon-echo technique. The method is sensitive to collisional velocity changes concerning both the total population ρ^0 and the alignment ρ^2 of the level. More specifically, it enables us to compare precisely the velocity changes associated with elastic scattering and with alignment-preserving scattering. This represents an improvement with regard to previous works. A detailed theoretical discussion of depolarizing collisions in laser spectroscopy is presented. A simplified density-matrix equation is derived under appropriate approximations. Stimulated photon-echo data for elastic scattering are interpreted within the limits of small-angle scattering in a long-range van der Waals potential; total elastic scattering cross sections are derived from comparison between experiment and calculation: $\sigma^{el}_{He}=220(20)$ Å^2, $\sigma^{el}_{Ne}=320(20)$ Å^2, $\sigma^{el}_{Xe}=1240(60)$ Å^2. Total rates for destruction of alignment are measured in an auxiliary standard photon-echo experiment; the corresponding cross sections are $\sigma^{(2)}_{He}=94(3)$ Å^2, $\sigma^{(2)}_{Ne}=123(7)$ Å^2, $\sigma^{(2)}_{Xe}=300(20)$ Å^2. Stimulated photon-echo data for depolarizing collisions are successfully compared with a calculation that we develop starting from a long-range anisotropic model potential.

I. INTRODUCTION

Detailed aspects of atomic and molecular collisions are revealed only through angular analysis of scattering processes and determination of differential cross sections. Crossed-beam experiments provide one with the most refined data. Among these, few experiments are concerned with inelastic collisions between neutrals and allow for the study of correlation between the center-of-mass motion and the change in internal state. Mention should be made of the crossed-beam determination of differential cross sections for collisional transfer between rotational levels in Na_2,[1] between Zeeman sublevels in metastable Ne($^3P_2$),[2] and between fine-structure levels in Na($3\,^2P$).[3] Such investigations require highly sophisticated techniques and generally concern ground states or long-lived metastable states of atoms and molecules. There have been some attempts to derive angular information on collisional processes through other methods such as nonlinear laser spectroscopy. Collision analysis as a function of the impact parameter has been attempted with promising results by studying collisional redistribution of light.[4] Depolarizing collisions (transfer between magnetic sublevels) may be regarded as the most elementary inelastic process on which nonconventional methods should be tested.

Depolarizing collisions have been mainly studied through measurements of the total decay rate γ^k for the k multipole.[5,6] Most of the works have been devoted to alkali-metal atoms and to group-IIb elements (Zn, Cd, and Hg) perturbed by noble gases. In the latter case the cross sections can be calculated with simple models for which the long-range van der Waals interaction dominates. Agreement with measured decay rates is generally good.[5] Some experimental information on the differential depolarizing cross sections should permit a further check of the validity of these models.

Nonlinear Doppler-free spectroscopic techniques are available in both the frequency and time domains. In the frequency domain, saturation spectroscopy,[7,8] polarization spectroscopy,[9,10] and optical double resonance[11–14] experiments have been set up in order to obtain some angular information in collisional studies. Through the determination of the collisional velocity change along the laser-beam direction, access is given to some average of the differential cross section among undetected degrees of freedom. The collisional inelastic processes which have been investigated through this method are the transfers between Zeeman sublevels (m-changing collisions, depolarizing collisions)[7–12] and between rotational levels.[13,14] Depolarizing-collision studies have led only to some qualitative indications for the existence of velocity changes during multipole-preserving collisions[8] or to some rough estimate of the smallness of such velocity changes.[7,10] Successful determination of velocity changes in inelastic processes has only been achieved in the case of rotational transfer in CO_2—foreign-gas collisions.[14]

More recently, nonlinear spectroscopic techniques in the time domain have proved adequate for studying collisional velocity changes. Various aspects of elastic collisions have been examined in photon-echo experiments. The two-pulse echo builds up from those optical coherences which have survived during a time interval which is twice the delay between the two laser pulses. Both internal phase memory and spatial phase memory are required for coherence preservation.[15] Thus the signal is sensitive to spatial phase destruction due to collisional velocity changes. The point is that collisions are undergone now by atomic coherence instead of level population. In other

words, one detects collisions which occur in a superposition state. Corresponding velocity changes have been measured in Li,[16] Na,[17] and Yb.[18] They have been shown to occur in the small-angle diffractive scattering region.[16] The three-pulse echo (stimulated photon echo) involves a periodic modulation inside the velocity distribution of an atomic level;[15,19] collisional velocity changes destroy this structure and thus contribute to signal relaxation. From signal-decay-rate measurements one has determined the collisional velocity changes due to diffractive or to classical scattering in a ground or an excited level.[19–21]

Thus far restricted to elastic scattering studies, the stimulated-photon-echo technique should be extended to the study of resonant (or quasiresonant) inelastic processes. Indeed, one may detect the collisional transfer of the velocity modulation from the initially perturbed level to an initially unperturbed one. In the present paper we illustrate this feature in the case of collisional transfer between degenerate Zeeman sublevels. Our experiment is performed in ytterbium vapor and allows for a detailed investigation of the classical elastic scattering and of depolarizing collisions in the $6s\,6p\ ^3P_1$ excited state. Velocity changes are measured for both processes. Information that we derive on differential cross sections for depolarizing collisions is used to check the standard calculations of the previously mentioned γ^k rates.

This paper is organized as follows. Section II is devoted to a general discussion of depolarizing collisions in laser spectroscopy and to derivation of a simplified density-matrix equation under appropriate approximations. The stimulated-photon-echo experiment is presented in Sec. III. The results for elastic and depolarizing collisions are discussed in Sec. IV. Section II may be read independently of Secs. III and IV and reference to results which are derived in Sec. II is clearly indicated when needed in Secs. III and IV.

II. DEPOLARIZING COLLISIONS IN LASER SPECTROSCOPY

A. Scattering amplitude

This subsection presents the main features of the semiclassical scattering amplitude which underlies our analysis of atomic-density-matrix relaxation in depolarizing collisions. Some characteristics of this picture already have been examined in a previous paper.[22]

An elastic collision scatters a plane wave with wave vector $\mathbf{K}$ in direction $\mathbf{r}(\theta,\phi)$, with an amplitude $f(\theta,\phi)$. In a depolarizing process the translational motion is still represented by the scattering of a plane wave. In addition, a change in the internal angular momentum must be described. Initial and final angular momenta are conveniently measured along initial and final relative-velocity directions, respectively. This is known as the helicity representation.[23] Thus the initial and final quantization axes are directed along the initial wave vector $\mathbf{K}$ and along the final internuclear vector $\mathbf{r}$, respectively. Helicity and body-fixed representations coincide in the final state. Connection between them is easily obtained in the initial state, since then $-\mathbf{r}$ is directed along the relative-velocity axis. The scattering amplitude in the helicity representation $f^{\rm hel}_{MM'}(\psi,\theta,\phi)$ may be written as[24]

$$f^{\rm hel}_{MM'}(\psi,\theta,\phi)=\frac{(-1)^{M-M'}}{2iK}\sum_J(2J+1)(S^J_{MM'}-\delta_{MM'})\times\left[D^J_{MM'}(\phi,\theta,\psi)\right]^*, \quad (1)$$

where $S^J_{MM'}$ is an S-matrix element, $D^J_{MM'}(\phi,\theta,\psi)$ is the rotation matrix of rank J, and (ϕ,θ,ψ) are the Euler angles of $\mathbf{r}$ with respect to $\mathbf{K}$. The internal angular momentum $\mathbf{j}$ and the relative orbital momentum $\mathbf{l}$ have been coupled into the total angular momentum $\mathbf{J}=\mathbf{l}+\mathbf{j}$ and the summation is over all allowed values of J. The depolarization amplitude exhibits a form which is very similar to that of the elastic amplitude:

$$f(\theta)=\frac{1}{2iK}\sum_l(2l+1)(e^{2i\eta_l}-1)P_l(\cos\theta), \quad (2)$$

where η_l is the phase shift of the l-labeled partial wave.

As long as the ratio $\lambda\!\!\!^{-}/a$ of the de Broglie wavelength to the potential dimension is small, a semiclassical picture holds for both depolarizing and elastic collisions. Then S-matrix elements may be calculated along classical paths.[22] In this picture the angular momentum $l\hbar$, which is greater than or equal to $Ka\hbar$, is supposed to be much larger than the momentum unit $\hbar$. As a consequence, $l\sim J$ and the exchange of angular momentum between $\mathbf{l}$ and $\mathbf{j}$ does not affect the classical paths along which $S^J_{MM'}$ is calculated. However, we shall see that the requisite of total angular momentum conservation is preserved in the form of the scattering amplitude.

Although the semiclassical S matrix is valid provided $\lambda\!\!\!^{-}\ll a$, this condition is not sufficient to regard the atoms as wave packets of dimension much smaller than the interaction domain. The more stringent condition $\sqrt{\lambda\!\!\!^{-}}\ll\sqrt{a}$ is needed in order to do so and its fulfillment is assumed in the following discussion.[25] Let us denote by l_θ the values of l which contribute efficiently to the sum in Eqs. (1) and (2). Two scattering-angle domains must be considered.

1. $l_\theta\theta\gg1$, $l\gg1$

In this region asymptotic expressions hold for $P_l(\cos\theta)$ and for $d^J_{MM'}(\theta)=D^J_{MM'}(0,\theta,0)$:

$$d^J_{MM'}(\theta)\simeq\frac{2}{\pi J\sin\theta}\sin\left[(J+\tfrac{1}{2}+M)\theta-\tfrac{1}{2}(M-M')\pi+\frac{\pi}{4}\right], \quad (3)$$

$$P_l(\cos\theta)\simeq\frac{2}{\pi l\sin\theta}\sin\left[(l+\tfrac{1}{2})\theta+\frac{\pi}{4}\right]. \quad (4)$$

The former expression is obtained by expression $d^J_{MM'}(\theta)$ in terms of Jacobi polynomials $P_{J-M}^{(M-M',M+M')}(\cos\theta)$ (Ref. 26) and then by using asymptotic expansions of these polynomials.[27] The latter expression results from $P_l(\cos\theta)=d^l_{00}(\theta)$. Both expressions exhibit a fast oscillation as a function of $l\theta$ or $J\theta$. The fast-varying phase in

$S^J_{MM'}$ (respectively $e^{2i\eta_l}$) combines with $J\theta$ (respectively $l\theta$). Then the sum over l or J may be evaluated using the stationary-phase approximation which reduces the sum to the contributions of the stationary-phase regions. The phase in Eq. (3) differs from its counterpart in Eq. (4) by an unimportant term $(M-M')\pi/2$ which does not modify the stationary-phase calculation. In the case of elastic scattering in a purely repulsive potential, the phase is stationary at $l=l_\theta$ which is unique for a given θ value and l_θ/K is equal to the classical impact parameter associated with classical scattering at θ. In addition $|f(\theta)|^2$ is equal to the classical elastic scattering differential cross section. When the potential function is not monotonic, several l values may contribute to scattering at θ. Then the ith contribution $f^i(\theta)$ to scattering amplitude arises from orbital momentum l^i_θ. It corresponds to the ith contribution $\sigma^i(\theta)=|f^i(\theta)|^2$ of scattering at impact parameter l^i_θ/K to the classical differential cross section. Clearly, interference effects between scattering-amplitude components $f^i(\theta)$ are lost in a classical cross section. In the depolarizing-collision semiclassical picture that we examined in a previous paper,[22] we considered the case of a simple potential $V_M(r)$ which is such that $|V_M(r)-V_{M\pm1}(r)|$ is a monotonic, decreasing function of r. Entering the collision region with a component M along $\mathbf{r}$, at an impact parameter J/K, the internal spin $\mathbf{j}$ rotates with regard to $\mathbf{r}$ until it is locked to $\mathbf{r}$ with a component M'', at an internuclear distance r_J. Then the spatial trajectory may depend on the M'' value in which locking has occurred. Finally, $\mathbf{j}$ decouples from $\mathbf{r}$ at distance $r_{JM''}$ and $\mathbf{j}$ rotates again with respect to $\mathbf{r}$. Let us assume in addition that $V_M(r)>0$ (purely repulsive potential). Then, the scattering amplitude at angle θ combines contributions from trajectories at different impact parameters $J^{M''}_\theta/K$ but each component $f^{M''}_{MM'}(\theta)$ may be decomposed as the product of the elastic scattering amplitude along the M''-labeled trajectory with the internal-state time-evolution matrix calculated along the classical M'' path. This picture could be presumably extended to scattering in nonmonotonic potentials with an increasing number of classical trajectories involved in scattering at angle θ. This semiclassical picture cannot apply if there is a sharp potential discontinuity or in an orbiting situation. Besides, one has to examine carefully trajectory coalescence, which occurs, for instance, in glory and rainbow effects.

The initial condition $l_\theta\theta\gg1$ expresses nothing but the fulfillment of the uncertainty-principle requirement by the impact parameter b_θ and by the associated final transverse momentum $P_t\sim\hbar K\theta$:

$$P_t b\sim\hbar l_\theta\theta\gg\hbar\ . \tag{5}$$

Indeed, a classical trajectory picture demands that l_θ and P_t be simultaneously measurable. We now examine what occurs in the region where this condition is not satisfied.

2. $l_\theta<1$, $l\gg1$

In this region[27]

$$\begin{aligned} &d^J_{MM'}(\theta)=J_{MM'}(J\theta)\ ,\\ &P_l(\cos\theta)=J_0((l+\tfrac{1}{2})\theta)\ . \end{aligned} \tag{6}$$

The stationary-phase approximation no longer applies for calculating the scattering amplitude and all l values such that $l>\theta^{-1}$ contribute to elastic scattering at θ. The wave nature of spatial motion appears and elastic scattering may be thought of as the diffraction of an incident plane wave, with de Broglie wavelength $\lambda\!\!\!^{-}=K^{-1}$, by an opaque screen sized to the dimension of the total cross section. The parallel between elastic and depolarizing collisions is not as straightforward as in Sec. II A 1.

While $P_l(\cos\theta)$ does not significantly differ from $d^J_{MM'}(\theta)$ when $l\theta\gg1$, a marked difference appears when $l\theta<1$ and $M\neq M'$. Then,

$$\begin{aligned} &\lim_{l\theta\to0}P_l(\cos\theta)=\lim_{l\theta\to0}d^J_{MM}(\theta)=1\ ,\\ &\lim_{l\theta\to0}d^J_{MM'}(\theta)=\delta_{MM'}\ . \end{aligned} \tag{7}$$

A classical mechanical interpretation is feasible when $J\gg j$. Orbital momentum l components along $\mathbf{K}$ and $\mathbf{r}$ equal zero. Thus components of total angular momentum $\mathbf{J}$ and of internal momentum $\mathbf{j}$ coincide along $\mathbf{K}$ and $\mathbf{r}$. The angle between $\mathbf{K}$ and $\mathbf{r}$ is $\theta\ll1$. Components of $\mathbf{J}$ along $\mathbf{K}$ and $\mathbf{r}$ are, respectively, $M=J\cos(\mathbf{J},\mathbf{K})$ and $M'=J\cos(\mathbf{J},\mathbf{r})$. Then, elementary geometrical arguments show that $|M-M'|$ cannot exceed $l\theta$. This means that $l\theta$ is the maximum angular momentum which can be transferred from $\mathbf{l}$ to $\mathbf{j}$ during a small-angle collision. Quantization of $M-M'$ requires that $M-M'=0$ or $|M-M'|\geq1$. Thus depolarization can be effective only if $l\theta>1$. In other words, collisional depolarization does not occur in the diffractive region. This picture relies on the conservation of the total angular momentum during the collision. It is complemented by the interpretation of $|d^J_{MM'}(\theta)|^2$ as the probability of finding a projection M' of $\mathbf{J}$ on the $\mathbf{r}$ axis, if it is known that the projection of $\mathbf{J}$ on $\mathbf{K}$ equals M.[28] It appears that $S^J_{MM'}$ and $d^J_{MM'}(\theta)$, respectively, represent the dynamics and the mechanics of the collision. The semiclassical scattering amplitude in the helicity representation may be introduced now into the density-matrix transport equation.

B. Density-matrix transport equation

In a gas cell the quantum-mechanical state of atoms in a definite level, with internal momentum j, within a small domain of position-velocity space around $(\mathbf{r},\mathbf{v})$ is most conveniently described by the density-matrix elements $\rho_{mm'}(\mathbf{r},\mathbf{v})$, where m and m' label magnetic sublevels and are taken along a fixed quantization axis $\mathbf{A}$. The transport equation which determines the collisional evolution of density-matrix elements of active atoms immersed in a perturber bath is given by[29]

$$\begin{aligned} \frac{\partial}{\partial t}\rho_{mm'}\bigg|_{\text{coll}} &= -\sum_{\substack{m''\\m'''}}\Gamma^{m''m'''}_{mm'}(\mathbf{v})\rho_{m''m'''}(\mathbf{r},\mathbf{v},\mathbf{t})\\ &\quad+\sum_{\substack{m''\\m'''}}\int d^3v'W^{m''m'''}_{mm'}(\mathbf{v}',\mathbf{v})\rho_{m''m'''}(\mathbf{r},\mathbf{v}',t)\ , \end{aligned} \tag{8}$$

where

$$\Gamma^{m''m'''}_{mm'}(\mathbf{v})=N\int d^3v_p\,W_p(\mathbf{v}_p)\times\left[\frac{2\pi\hbar}{i\mu}[f_{m''m}(\mathbf{u},\mathbf{u},\mathbf{A})\delta_{m'm'''}-f^*_{m'''m'}(\mathbf{u},\mathbf{u},\mathbf{A})\delta_{mm''}]\right] \quad (9)$$

and

$$W^{m''m'''}_{mm'}(\mathbf{v}',\mathbf{v})=N\int d^3u\int d^3u'\delta(\mathbf{v}'-\mathbf{v}-\mathbf{Y})W_p(\mathbf{v}-\mathbf{u}'+\mathbf{Y})\times\delta(u-u')u^{-1}f_{m''m}(\mathbf{u}',\mathbf{u},\mathbf{A})\times f^*_{m'''m'}(\mathbf{u}',\mathbf{u},\mathbf{A}), \quad (10)$$

where $\mathbf{u}$ is the relative velocity between active atom and perturber, $W_p(\mathbf{v}_p)$ is the perturber equilibrium velocity distribution, $\mathbf{Y}=(\mu/m)(\mathbf{u}'-\mathbf{u})$, N is the perturber density, and $f_{m'm}(\mathbf{u}',\mathbf{u},\mathbf{A})$ is the scattering amplitude from $m',\mathbf{u}'$ to $m,\mathbf{u}$, with quantization along the fixed axis $\mathbf{A}$. This scattering amplitude may be expressed as a function of the previously defined scattering amplitude in the helicity representation:

$$f_{mm'}(\mathbf{u}',\mathbf{u},\mathbf{A})=\sum_{M,M'}[D^j_{mM}(R')]^*D^j_{m'M'}(R)f^{\rm hel}_{MM'}(\mathbf{u}',\mathbf{u}), \quad (11)$$

where $R=(\phi_{u'},\theta_u,0)$, $R'=(\phi_{u'},\theta_{u'},0)$ and ϕ_u and θ_u are the polar angles of $\mathbf{u}$ with respect to $\mathbf{A}$.

In traditional optical-pumping experiments in which depolarizing collisions have been studied,[5,6] neither the vapor excitation nor the signal detection are velocity selective. Due to isotropy in the velocity space, the atomic-density-matrix components in a basis of the rotation-group irreducible tensorial operators remain uncoupled during their relaxation in depolarizing collisions.[30] Expansion on this basis still proves useful when isotropy is lost. One defines[30]

$$\rho^k_q(\mathbf{r},\mathbf{v},t)=\sum_{m,m'}(-1)^{j-m'}\begin{pmatrix}j&k&j\\-m'&q&m\end{pmatrix}\times(2k+1)^{1/2}\rho_{mm'}(\mathbf{r},\mathbf{v},t). \quad (12)$$

Substitution of Eq. (11) in Eqs. (8)—(10), and use of elementary properties of D matrices, lead to

$$\frac{\partial}{\partial t}\rho^k_q\bigg|_{\rm coll}=-\sum_{k',q'}\left[\Gamma^{k'k}_{q'q}(\mathbf{v})\rho^{k'}_{q'}(\mathbf{v})+\int W^{k'k}_{q'q}(\mathbf{v}',\mathbf{v})\rho^{k'}_{q'}(\mathbf{v}')d\mathbf{v}'\right], \quad (13)$$

where

$$\Gamma^{k'k}_{q'q}(\mathbf{v})=N\int d^3v_p\,W_p(\mathbf{v}_p)\sum_{M,c}(2k+1)^{1/2}(2k'+1)^{1/2}(2c+1)\begin{pmatrix}j&j&c\\M&-M&0\end{pmatrix}\frac{2\pi\hbar}{i\mu}\begin{Bmatrix}k&k'&c\\j&j&j\end{Bmatrix}\times[D^c_{Q0}(R)]^*(-1)^{M+j}\left[(-1)^q\begin{pmatrix}k'&k&c\\q'&-q&Q\end{pmatrix}f^{\rm hel}_{MM}(u,0)-(-1)^{q'}\begin{pmatrix}k&k'&c\\-q&q'&Q\end{pmatrix}[f^{\rm hel}_{MM}(u,0)]^*\right] \quad (14)$$

and

$$W^{k'k}_{q'q}(\mathbf{v}',\mathbf{v})=N\int\int d^3u\,d^3u'\delta(\mathbf{v}'-\mathbf{v}-\mathbf{Y})W_p(\mathbf{v}'_p)\delta(u-u')u^{-1}\times\sum\begin{pmatrix}k'&k&c\\-q'&q&\gamma\end{pmatrix}\begin{pmatrix}k'&k&c\\Q'&-P&\gamma'\end{pmatrix}\begin{pmatrix}j&k&j\\M&Q&-M'\end{pmatrix}\begin{pmatrix}j&k'&j\\M''&Q'&-M'''\end{pmatrix}\times(2k+1)^{1/2}(2k'+1)^{1/2}(2c+1)(-1)^{q'+Q'+M+M''}[D^c_{\gamma\gamma'}(R')]^*D^k_{-P-Q}(R'')\times f^{\rm hel}_{M''M}(u,R'')[f^{\rm hel}_{M'''M'}(u,R'')]^*, \quad (15)$$

where $R''=R'^{-1}R$, $R=(\phi,\theta,\psi)$.

The average of Eq. (13) over active-atom velocity releases coupling between multipoles and leads to the familiar relaxation equation which occurs in the analysis of traditional optical-pumping experiments.[30] The corresponding k-multipole decay rate is given by

$$\gamma^k=\sum_{k',q'}\int d^3v\,W(\mathbf{v})\left[\Gamma^{k'k}_{q'q}(\mathbf{v})-\int W^{k'k}_{q'q}(\mathbf{v},\mathbf{v}')d^3v'\right]=\pi N\sum\begin{pmatrix}j&k&j\\M&Q&-M'\end{pmatrix}\begin{pmatrix}j&k&j\\M''&Q'&-M'''\end{pmatrix}\begin{pmatrix}J&k&J'\\M''&Q'&-M'''\end{pmatrix}\begin{pmatrix}J&k&J'\\M&Q&-M'\end{pmatrix}(2J+1)(2J'+1)\times\int d^3u\,W_r(\mathbf{u})\frac{u}{K^2}[\delta_{M''M}\delta_{M'M'''}-S^J_{M''M}(S^{J'}_{M'''M})^*], \quad (16)$$

where $W_r(\mathbf{u})$ and $W(\mathbf{v})$ are, respectively, the relative-velocity distribution and the active-atom velocity distribution.

In velocity-selective experiments, multipoles are coupled as indicated by Eqs. (14) and (15). However, approximations which are compatible with our experimental conditions decouple the multipoles and enlighten the connection between the k-multipole decay rate γ^k and the collision kernel $W^{k'k}_{q'q}(\mathbf{v}',\mathbf{v})$.

1. Isotropic relative-velocity distribution

This approximation requires that $m_p \ll m$. When this condition is fulfilled, $W_p(\mathbf{v}_p)$ may be replaced by the relative-velocity distribution function $W_r(\mathbf{u}')$ in $W^{k'k}_{q'q}(\mathbf{v}',\mathbf{v})$. Integration variables are changed from $\mathbf{u},\mathbf{u}'$ to $\mathbf{Y},\mathbf{u}'$. Integration over $\Omega_{\mathbf{u}'}$ leads to

$$W^{k'k}_{q'q}(\mathbf{v}',\mathbf{v}) = N\int d^3Y\, d^3u'\,\delta(\mathbf{v}'-\mathbf{v}-\mathbf{Y})W_r(\mathbf{u}') \times\delta(u-u')u^{-1}\delta_{kk'}\delta_{qq'}(d\sigma^k/d\Omega) = W^k(\mathbf{v}',\mathbf{v})\delta_{kk'}\delta_{qq'}\,, \tag{17}$$

where

$$\frac{d\sigma^k(\theta)}{d\Omega} = \sum_{\substack{M,M'\\M'',M'''}} \begin{pmatrix} j & k & j\\ M & Q & -M'\end{pmatrix}\begin{pmatrix} j & k & j\\ M'' & Q' & -M'''\end{pmatrix} \times(-1)^{M'''-M'}[D^k_{Q'Q}(R'')]^* \times f^{\rm hel}_{M''M}(u,R'')[f^{\rm hel}_{M'''M'}(u,R'')]^*\,. \tag{18}$$

An analogous procedure for $\Gamma^{k'k}_{q'q}(\mathbf{v})$ leads to

$$\Gamma^{k'k}_{q'q}(\mathbf{v}) = \delta_{kk'}\delta_{qq'}N\int d^3u\; W_r(\mathbf{u})\frac{1}{(2j+1)}\frac{4\pi\hbar}{\mu} \times\sum_M \mathrm{Im}f^{\rm hel}_{MM'}(u,0)\,. \tag{19}$$

The elastic scattering cross section in a degenerate level is

$$\frac{d\sigma_{\rm el}}{d\Omega} = \frac{1}{(2j+1)}\sum_{M,M'}\frac{d\sigma_{MM'}}{d\Omega}\,, \tag{20}$$

where $\sigma_{MM'}$ is the scattering cross section for collisional transition from M to M'. Equation (18) leads to

$$\frac{d\sigma^{(0)}}{d\Omega} = \frac{d\sigma_{\rm el}}{d\Omega} \tag{21}$$

and, according to the optical theorem, Eq. (19) reduces to

$$\Gamma^{k'k}_{q'q}(\mathbf{v}) = \gamma^{\rm el}\delta_{kk'}\delta_{qq'}\,, \tag{22}$$

where

$$\gamma^{\rm el}(\mathbf{v}) = N\int d^3u\; uW_r(\mathbf{u})\sigma_{\rm el}(u)\,. \tag{23}$$

Finally, Eq. (13) reduces to

$$\left.\frac{\partial}{\partial t}\rho^k_q\right|_{\rm coll} = -\gamma^{\rm el}(\mathbf{v})\rho^k_q + \int W^k(\mathbf{v}',\mathbf{v})\rho^k_q d^3v'\,. \tag{24}$$

An analogy with the elastic scattering Boltzmann transport equation[29] suggests that $d\sigma^k/d\Omega$ be regarded as the k-multipole-preserving differential scattering cross section.

2. Isotropic small-angle scattering

Let us assume that short-range interaction does not contribute to forward scattering and that in the long-range region $|V_M(b)-V_{M'}(b)| \ll \hbar u/b$ for impact-parameter values which correspond to small-angle scattering. In this region no depolarization occurs and

$$f^{\rm hel}_{MM'}(u,R'') \simeq f(u,\theta_{\mathbf{u},\mathbf{u}'})\delta_{MM'} \quad \text{with } \theta_{\mathbf{u},\mathbf{u}'} \ll 1\,. \tag{25}$$

Substitution of Eq. (25) in Eqs. (14) and (15) leads to

$$\Gamma^{k'k}_{q'q}(\mathbf{v}) = \delta_{kk'}\delta_{qq'}\gamma^{\rm el}(\mathbf{v})\,, \tag{26}$$

$$W^{k'k}_{q'q}(\mathbf{v}',\mathbf{v}) = \delta_{kk'}\delta_{qq'}W^k(\mathbf{v}',\mathbf{v}) \quad \text{with } \frac{m}{\mu}|\mathbf{v}'-\mathbf{v}| \ll 1\,, \tag{27}$$

where

$$\gamma^{\rm el}(\mathbf{v}) = N\int d^3u\; W_p(\mathbf{u}-\mathbf{v})\frac{4\pi h}{\mu}\mathrm{Im}f(u,0) \tag{28}$$

and

$$W^k(\mathbf{v}',\mathbf{v}) = N\int d^3u\, d^3u'\,\delta(\mathbf{v}'-\mathbf{v}-\mathbf{Y})W_p(\mathbf{u}'-\mathbf{v}') \times\delta(u-u')u^{-1}|f(u,R'')|^2\,. \tag{29}$$

$W^k(\mathbf{v}',\mathbf{v})$ is indeed k independent and the k label is only used here for notational consistency.

3. Common trajectory for different M sublevels

We assume that the difference between the scattering potentials for different magnetic substates is small enough that the spatial trajectories do not depend on the previously defined M'' momentum which characterizes the internal state when $\mathbf{j}$ is locked to $\mathbf{r}$ (cf. Sec. II A and Ref. 22). In the classical scattering region (i.e., when $l_\theta\theta \gg 1$) the dynamical factor in Eq. (16) can be written as[22]

$$\delta_{M'''M'}\delta_{M''M} - (S^{J'}_{M'''M'})^* S^J_{M''M} = \delta_{M'''M'}\delta_{M''M} - [U^J_{-M'''M'}(-\infty,+\infty)]^* U^J_{-M''M}(-\infty,+\infty)\exp\frac{i}{\hbar} \times\int_0^\infty dt\,[V_{-M'''}(r_J(t)) + V_{M'}(r_J(t)) - V_{-M''}(r_J(t)) - V_M(r_J(t))]\exp[-i(J'-J)\theta]\,, \tag{30}$$

where $U^J_{-M''M}(-\infty,+\infty)$ is the time-evolution operator of internal state which is evaluated along trajectory $r_J(t)$ at impact parameter $J\hbar/\mu u$. Then we replace two 3-j symbols in Eq. (16) by their asymptotic expressions for large J values:[28]

$$\begin{pmatrix} J & J' & k \\ M'' & -M''' & Q' \end{pmatrix}\begin{pmatrix} J & J' & k \\ M & -M' & Q \end{pmatrix} \simeq \frac{(-1)^{M'''-M'}}{(2J'+1)} d^k_{(J'-J)Q'}\left(\frac{\pi}{2}\right) d^k_{(J'-J)Q}\left(\frac{\pi}{2}\right) . \quad (31)$$

In rotations of angle α and β around axis $0y$ and $0z$, respectively, the rotation operators which act on the eigenvectors $|IM\rangle$ of operators I^2 and I_z are denoted, respectively, $e^{-iI_y\alpha}$ and $e^{-iI_z\beta}$. One can verify that

$$e^{i\pi I_z/2}e^{-iI_y\theta}e^{i\pi I_z/2} = e^{-i\pi I_y/2}e^{iI_z\theta}e^{i\pi I_y/2} . \quad (32)$$

Using this identity and combining $\exp[-i(J'-J)\theta]$ in Eq. (30) with Eq. (31) we obtain

$$\sum_{J'}(2J'+1)\begin{pmatrix} J & J' & k \\ M'' & -M''' & Q' \end{pmatrix} \times \begin{pmatrix} J & J' & k \\ M & -M' & Q \end{pmatrix} e^{-i(J'-J)\theta} \simeq (-1)^{M'''-M'} e^{-i\pi(Q'-Q)/2} d_{Q'Q}(\theta) . \quad (33)$$

Thus γ^k takes the form

$$\gamma^k = \pi N \sum_J (2J+1) \int \frac{d^3u}{K^2} W_r(\mathbf{u}) P^k(J,u) , \quad (34)$$

where

$$P^k(J,u) = \sum_{\substack{M,M' \\ M'',M'''}} \begin{pmatrix} j & k & j \\ M & Q & -M' \end{pmatrix}\begin{pmatrix} j & k & j \\ M'' & Q' & -M''' \end{pmatrix}(-1)^{M'''-M'} e^{-i\pi(Q'-Q)/2} \times \left[\delta_{MM''}\delta_{M'M'''} - [U^J_{-M'''M'}(-\infty,+\infty)]^* U^J_{-M''M}(-\infty,+\infty)\exp\frac{i}{\hbar} \times \int_0^\infty dt[V_{-M'''}(r_J(t)) + V_{M'}(r_J(t)) - V_{-M''}(r_J(t)) - V_M(r_J(t))]d^k_{Q'Q}(\theta)\right] . \quad (35)$$

Changing the summation over J into an integral over b we obtain

$$\gamma^k = N \int 2\pi b db \int d^3u\, W_r(u) P^k(Kb,u) . \quad (36)$$

Thus $P^k(Kb,u)$ appears to be the destruction probability of multipole k along the classical trajectory which corresponds to impact parameter b and scattering angle θ. It should be noticed that different trajectories scattering into the same scattering angle θ cannot interfere since J and J' in Eq. (16) differ at most by k.

4. *Single trajectory at scattering angle θ*

We assume that a single angular momentum J_θ can contribute to scattering at angle θ. As already mentioned in Sec. II A this assumption corresponds to a monotonic potential curve. In the frame of this approximation the product $[f^{\text{hel}}_{M'''M'}(R'')]^* f^{\text{hel}}_{M''M}(R'')$ in Eq. (18) is given by[22]

$$[f^{\text{hel}}_{M'''M'}(R'')]^* f^{\text{hel}}_{M''M}(R'') = \frac{J_\theta}{K^2\pi\sin\theta\left|\frac{d\theta}{dJ_\theta}\right|}[U^{J_\theta}_{-M'''M'}(-\infty,+\infty)]^* U^{J_\theta}_{-M''M}(-\infty,+\infty) \times \exp\frac{i}{\hbar}\int_0^\infty dt[V_{-M'''}(r_{J_\theta}(t)) - V_{-M''}(r_{J_\theta}(t)) + V_{M'}(r_{J_\theta}(t)) - V_M(r_{J_\theta}(t))]\exp\left[-i(Q'-Q)\frac{\pi}{2}\right] . \quad (37)$$

Substitution in Eq. (18) and comparison with Eq. (35) leads to

$$\frac{d\sigma^k}{d\Omega} = \frac{d\sigma^{(0)}}{d\Omega}[1 - P^k(Kb,u)] \quad (38)$$

which expresses the differential cross section for any multipole in terms of the elastic scattering cross section $d\sigma^{(0)}/d\Omega$ and of the multipole destruction probability along the corresponding classical trajectory. Thus we finally obtain

$$W^k(\mathbf{v}',\mathbf{v}) = W^{(0)}(\mathbf{v}',\mathbf{v}) - N\int d^3Y d^3u' \delta(\mathbf{v}'-\mathbf{v}-\mathbf{Y}) \times W_r(\mathbf{u}')\delta(u-u')u^{-1} \times \frac{d\sigma^{(0)}}{d\Omega} P^k(J_\theta,u) . \quad (39)$$

When the single-trajectory approximation breaks down, i.e., when several trajectories contribute to scattering at angle θ, interference terms appear in the product of scattering amplitudes and Eq. (38) is no longer valid. However, the interference pattern is velocity dependent and we guess that interference features are washed out by velocity averaging in $W^k(\mathbf{v}',\mathbf{v})$ which is the quantity of experimental interest. Then the product $(d\sigma^{(0)}/d\Omega)P^k(J\theta,u)$ in Eq. (39) should be replaced by a sum over the contributions from different impact parameters J^i_θ/K which contribute to scattering at angle θ. Velocity averaging is also expected to enable us to ignore singularities which may occur when trajectories coalesce.[31]

Generally, velocity-selective laser techniques only select the velocity component which lies along the laser-beam direction. In the following we assume that transverse motion is not affected by the perturbation which is produced by the laser within the axial (or longitudinal) velocity distribution. This separation enables us to write

$$\rho^k(\mathbf{v})=\rho^k(v_z)W(\mathbf{v}_\perp) \tag{40}$$

and

$$\left.\frac{\partial\rho^k_q(v_z)}{\partial t}\right|_{\text{coll}}=-\sum_{k',q'}\left[\Gamma^{k'k}_{q'q}(v_z)\rho^{k'}_{q'}(v_z)-\int W^{k'k}_{q'q}(v_z',v_z)\rho^{k'}_{q'}(v_z')dv_z'\right], \tag{41}$$

where

$$\Gamma^{k'k}_{q'q}(v_z)=\int\Gamma^{k'k}_{q'q}(\mathbf{v})W(\mathbf{v}_\perp)d\mathbf{v}_\perp \tag{42}$$

and

$$W^{k'k}_{q'q}(v_z',v_z)=\int W^{k'k}_{q'q}(\mathbf{v}',\mathbf{v})W(\mathbf{v}_\perp')d\mathbf{v}_\perp'd\mathbf{v}_\perp\ . \tag{43}$$

III. STIMULATED PHOTON ECHO IN YTTERBIUM VAPOR

A. Formation and relaxation of the echo

Stimulated photon echo (SPE) is produced by a three-pulse excitation sequence as illustrated in Fig. 1. In our case the laser pulses and the echo are copropagating. Concerning other geometries for phase matching as well as detailed calculations of the SPE signal we refer to papers by Hartmann and co-workers.[15,19] The first two pulses are resonant with the a-b transition and are separated by a time interval t_{12}. The third pulse is resonant with the b-c transition and is applied at a delay t_{23} after the second pulse. Interaction between the atomic vapor and the first two pulses produces a sinusoidal modulation (Fig. 1) in the longitudinal velocity distribution of level b; the modulation period is $\delta v_z=\lambda_1/t_{12}$ where λ_1 is the wavelength of the a-b transition.[15,19,32] The optical coherence ρ_{bc} is built up from this modulation by the third pulse and the dipoles rephase to emit the echo at a time $t_e=(\omega_1/\omega_2)t_{12}$ after this pulse. Echo formation involves three different atomic quantities during the excitation sequence (Fig. 1). The initial excitation memory is

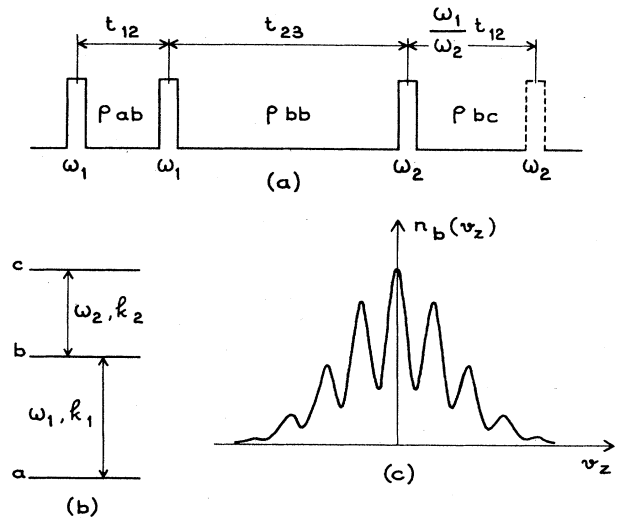

FIG. 1. (a) Light pulse sequence and (b) level scheme in a SPE experiment. (c) Modulation in the velocity distribution of level b after the first two pulses.

first transmitted by the optical coherence ρ_{ab} between the first two pulses, then by the modulation which survives in level b between the second and the third pulses, and finally by the coherence ρ_{bc} after the third pulse.

During the time interval t_{23}, relaxation of the echo results not only from depopulation of level b by spontaneous emission and by inelastic (state-changing) collisions but also from destruction of the modulation in velocity space by elastic (velocity-changing) collisions. The echo signal is due to the atoms which have not undergone velocity changes Δv_z larger than the modulation period. Let $2\Gamma_b(t_{12})$ be the contribution of elastic collisions to the relaxation rate of the echo signal during the time interval t_{23}. The echo signal is proportional to the velocity-modulated part of the level-b population $\tilde{\rho}_{bb}$ at time $t=t_3$:

$$\tilde{\rho}_{bb}(k_1t_{12})=\int\rho_{bb}(v_z)\cos(k_1v_zt_{12})dv_z\ . \tag{44}$$

$\tilde{\rho}_{bb}(k_1t_{12})$ is just the Fourier component of $\rho_{bb}(v_z)$ corresponding to a modulation period $\delta v_z=(k_1t_{12})^{-1}$.

Let us consider the case of transform-limited laser pulses which coherently excite a velocity domain $W_L(v_z)$ around v_L. The corresponding expression for the relaxation rate $\Gamma_b(t_{12})$ is approximately

$$\Gamma_b(t_{12})=\int W_L(v_z)\gamma^{\text{el}}(v_z)dv_z-\int W(v_z',v_z)W_L(v_z)\cos[k_1t_{12}(v_z'-v_z)]\times dv_z'dv_z\ , \tag{45}$$

where $W_z(v_z',v_z)$ is the one-dimensional kernel and $\gamma^{\text{el}}(v_z)=\int W(v_z,v_z')dv_z'$ is the elastic collision rate.

For sequences of non-transform-limited, mutually incoherent laser pulses of duration τ_L, each spectral element i with bandwidth $\sim(1/\tau_L)$ coherently excites a velocity domain $\Delta v\sim 1/k_1\tau_L$ centered at a particular velocity

$v_L^i - (\omega_i - \omega_1)/k_1$. Provided that $1/\tau_L$ is smaller than the Doppler width $\Delta\omega_D$, the observed signal is the incoherent superposition of elementary signals obtained from these different velocity domains. The relaxation rate associated with each domain i is $\Gamma_b(v_L^i, t_{12})$, obtained from Eq. (45) by taking for $W_L(v_z)$ a velocity distribution (distribution width $\sim 1/k_1\tau_L$) centered at v_L^i. If the spectral distribution and the spatial distribution of the energy in the laser pulses are not perfectly known, one cannot precisely determine $W_L(v)$ and $\Gamma(t_{12})$, whether pulses are transform limited or not, except when $1/\tau_L$ is much larger than the Doppler width; then $W_L(v_z) = W(v_z)$. However, simplification occurs when the perturber mass m_p is much smaller than the active-atom mass m. Then the relative-velocity distribution is nearly independent of the active-atom axial velocity and (see Appendix B)

$$W(v_z', v_z) \simeq W(0, v_z - v_z') = W(0, \Delta v_z) ,$$
$$\gamma^{\rm el}(v_z) \simeq \gamma^{\rm el}(0) = \gamma^{\rm el} . \tag{46}$$

Under this assumption, the relaxation rate $\Gamma_b(t_{12})$ has the simple expression currently used in SPE works:

$$\Gamma_b(t_{12}) \simeq \gamma^{\rm el} - \int W(0, \Delta v_z)\cos(k_1 \Delta v_z t_{12}) d(\Delta v_z) . \tag{47}$$

When $k_1 \Delta v_z t_{12} \ll 1$, velocity changes do not participate in the decay rate $\Gamma_b(t_{12})$ since, as $\cos(k_1 \Delta v_z t_{12}) \sim 1$, the departure term $\gamma^{\rm el} = \int W(0, \Delta v_z) d(\Delta v_z)$ and the restitution term balance each other. When $k_1 \Delta v_z t_{12} \gg 1$, contributions to the restitution term average to zero. Except for an additional constant, $\Gamma_b(t_{12})$ is the Fourier transform of the collision kernel $W(\Delta v_z)$. When Eqs. (46) do not hold, the above expression of the modulation relaxation rate (elastic collision contribution), $\Gamma_b(t_{12})$, is not correct; the correction factor, depending upon $\beta = m_p/m$, has been estimated in Appendix B when the coherent spectral width of the pulse is much larger than the Doppler width.

Up to now, formation and relaxation of the stimulated echo signal have been discussed without considering Zeeman degeneracy of levels and laser-beam polarization, so that we were concerned with the population in level b only. In a real situation we create a population ρ^0 in level b but, possibly also, orientation ρ^1, alignment ρ^2, and higher-order multipoles according to J values and to beam polarizations.

Our experiment has been performed with Yb atoms using levels $6s^2\,{}^1S_0$, $6s6p\,{}^3P_1$, and $6s7s\,{}^3S_1$ as levels a, b, and c, respectively [Fig. 2(a)]. The laser beams are linearly polarized and the echo is detected in the same linear polarization as the third laser pulse. Polarization of the first two pulses is either perpendicular [Fig. 2(b)] or parallel [Fig. 2(c)] to that of the third pulse. In the latter case (referred to as the parallel-polarization configuration) the signal only appears when depolarizing (m-state changing) collisions occur. The previously reported measurements[21] had been performed using the crossed-polarization configuration [Fig. 2(b)].

To give a correct expression for relaxation of the echo signals $I_\perp$ (crossed polarizations) and $I_{||}$ (parallel polarizations) it is more convenient to choose the polarization of

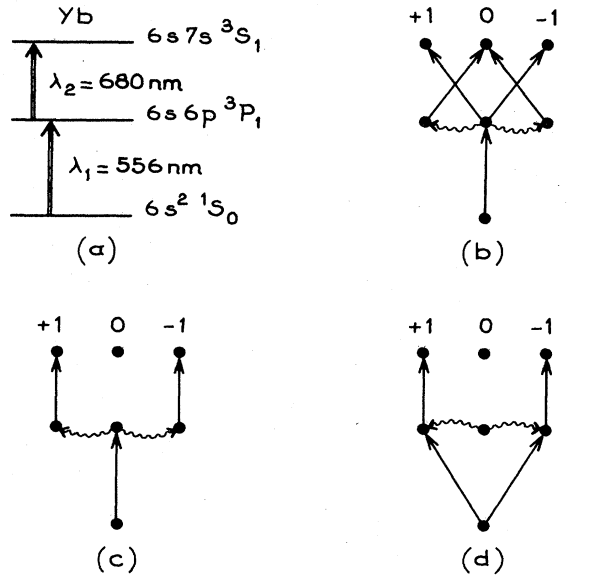

FIG. 2. (a) Level scheme and [(b)—(d)] beam polarizations for SPE experiment in ytterbium. Wavy arrows represent collisional transfer between Zeeman sublevels.

the third pulse (which is also the direction of the polarization for detection of the echo) as the quantization axis [Figs. 2(c) and 2(d)]. Let us define a density matrix $\tilde{\rho}$ for level b by

$$\tilde{\rho}(k_1 t_{12}) = \int_{-\infty}^{+\infty} \rho_b(v_z)\cos(k_1 v_z t_{12}) dv_z . \tag{48}$$

$\tilde{\rho}$ is just the velocity-modulated part of the level-b density matrix with a modulation period equal to $(k_1 t_{12})^{-1}$.

The echo signal is proportional to $|\rho_{bc}(t_e)|^2$ [Fig. 1(a)] and ρ_{bc} is proportional to the velocity-modulated part of the level-b population at time $t = t_3$, i.e., in our particular case [Figs. 2(c) and 2(d)], $I \propto |\tilde{\rho}_{++}(t_3) + \tilde{\rho}_{--}(t_3)|^2$. In the absence of depolarizing collisions we have $\tilde{\rho}_{++} = \tilde{\rho}_{--} \neq 0$ in the crossed-polarization configuration [Fig. 2(d)] while we have $\tilde{\rho}_{++} = \tilde{\rho}_{--} = 0$ in the parallel-polarization configuration [Fig. 2(c)].

The density matrix $\tilde{\rho}$ can be expanded upon an irreducible tensor basis T_q^k (Sec. II, Ref. 30); the corresponding matrix elements $\tilde{\rho}_0^k$ are related to those in the mm' basis $\tilde{\rho}_{mm'}$. The relations of interest in our case are

$$\tilde{\rho}_{00} = \frac{1}{\sqrt{3}}\tilde{\rho}_0^0 - \frac{\sqrt{2}}{\sqrt{3}}\tilde{\rho}_0^2 ,$$
$$\tilde{\rho}_{++} + \tilde{\rho}_{--} = \frac{2}{\sqrt{3}}\tilde{\rho}_0^0 + \frac{\sqrt{2}}{\sqrt{3}}\tilde{\rho}_0^2 \tag{49}$$

or conversely

$$\tilde{\rho}_{00} + \tilde{\rho}_{++} + \tilde{\rho}_{--} = \sqrt{3}\rho_0^0 ,$$
$$\tilde{\rho}_{++} + \tilde{\rho}_{--} - 2\tilde{\rho}_{00} = \sqrt{6}\rho_0^2 . \tag{50}$$

ρ^0 is a scalar and is proportional to the *total* population of the $J=1$ level, ρ^1 (which is zero in our case) behaves as a dipole and is referred to as orientation, and ρ^2 behaves as a quadrupole and is referred to as alignment.

The velocity-modulated population $\tilde{\rho}^0$ and alignment

$\tilde{\rho}^2$ are created by the first two pulses and then relax during the time interval t_{23} between the second and the third pulses. At time $t=t_2$, just after the second pulse, in the crossed-polarization configuration we get $\tilde{\rho}_{++}=\tilde{\rho}_{--}=\tilde{N}_0/2$ and $\tilde{\rho}_{00}=0$ and thus $\tilde{\rho}_0^0=\tilde{N}_0/\sqrt{3}$ and $\tilde{\rho}_0^2=\tilde{N}_0/\sqrt{6}$. Similarly, in the parallel configuration we get, at $t=t_2$, $\tilde{\rho}_{00}=\tilde{N}_0$ and $\tilde{\rho}_{++}=\tilde{\rho}_{--}=0$ and thus $\tilde{\rho}_0^0=\tilde{N}_0/\sqrt{3}$ and $\tilde{\rho}_0^2=-2\tilde{N}_0/\sqrt{6}$.

Following the discussion of Sec. II B we may write

$$W_{q'q}^{k'k}(v_z,v_z')=\delta_{kk'}\delta_{qq'}W^k(v_z',v_z)\ , \tag{51}$$

$$\Gamma_{q'q}^{k'k}(v_z)=\delta_{kk'}\delta_{qq'}\gamma^{\mathrm{el}}(v_z) \tag{52}$$

provided one of the following two conditions is fulfilled: (i) isotropic relative-velocity distribution (c.f. Sec. II B 1) and (ii) isotropic scattering in the $|v_z'-v_z|$-explored domain (cf. Sec. II B 2). In these expressions, γ^{el} is the total rate of elastic collisions which affect the *total population* of level b; W^k is the collision kernel corresponding to the restitution of the k multipole in level b. According to Eqs. (17), (23), (28), (29), (42), and (43), γ^{el} is connected to $W^{(0)}$ by $\gamma^{\mathrm{el}}(v_z)=\int W^{(0)}(v_z,v_z')dv_z'$. Then Eq. (13) reduces to

$$\left.\frac{\partial\rho_q^k}{\partial t}\right|_{\mathrm{coll}}=-\gamma^{\mathrm{el}}(v_z)\rho_q^k(v_z)+\int W^k(v_z',v_z)\rho_q^k(v_z')dv_z'\ . \tag{53}$$

If we also assume that Eq. (46) holds for population ($k=0$) and alignment ($k=2$), the time evolution (for $t_2\leq t\leq t_3$) of the modulated part of the population $\tilde{\rho}^0$ and of the alignment is described by

$$\begin{aligned}\tilde{\rho}_0^0(t)&=\tilde{\rho}_0^0(t_2)\exp[-\Gamma_b^{(0)}(t_{12})(t-t_2)]\ ,\\ \rho_0^2(t)&=\rho_0^2(t_2)\exp[-\Gamma_b^{(2)}(t_{12})(t-t_2)]\ ,\end{aligned} \tag{54}$$

where

$$\Gamma_b^k(t_{12})=\gamma^{\mathrm{el}}(0)-\int W^k(0,\zeta_z)\cos(k_1\zeta_z t_{12})d\zeta_z\ . \tag{55}$$

The total rate for collisional destruction of a k multipole is $\gamma^k=\Gamma_b^k(0)$; we have $\Gamma_b^{(0)}(0)=\gamma^{(0)}=0$. The SPE signal cannot be obtained for very small t_{12} since the existence of the modulation requires that $t_{12}>(\Delta\omega_d)^{-1}$; γ^k cannot be measured directly in a SPE experiment.

The echo signals $I_\perp$ and $I_{||}$, corresponding, respectively, to perpendicular- and to parallel-polarization settings, are expressed as

$$\begin{aligned}\left[\frac{I_\perp}{I_\perp^0}\right]^{1/2}&=\exp\left[-\left[\gamma_{ab}^{\mathrm{coll}}+\frac{\omega_1}{\omega_2}\gamma_{bc}^{\mathrm{coll}}\right]t_{12}\right]\exp[-\Gamma_b^{(0)}(t_{12})t_{23}]\tfrac{1}{3}(2+\exp\{-[\Gamma_b^{(2)}(t_{12})-\Gamma_b^{(0)}(t_{12})]t_{23}\})\exp(-\gamma_{\mathrm{inel}}t_{23})\ ,\\ \left[\frac{I_{||}}{I_\perp}\right]^{1/2}&=(2-2\exp\{-[\Gamma_b^{(2)}(t_{12})-\Gamma_b^{(0)}(t_{12})]t_{23}\})/(2+\exp\{-[\Gamma_b^{(2)}(t_{12})-\Gamma_b^{(0)}(t_{12})]t_{23}\})\ .\end{aligned} \tag{56}$$

γ_{inel} is the rate for inelastic (quenching) collisions in level b; $\gamma_{ab}^{\mathrm{coll}}$ ($\gamma_{bc}^{\mathrm{coll}}$) is the collisional relaxation rate for the atomic coherence ρ_{ab} (ρ_{bc}). $I_\perp^0$ is the echo signal at zero perturber pressure.

In our experiment an *isotropic relative-velocity distribution* may be reasonably assumed for collisions between Yb and light perturbers (He and Ne). The smallness of the signal ratio $I_{||}/I_\perp$ in the case of Yb-Xe collisions supports this assumption of *isotropic scattering* in the $(v_z'-v_z)$-explored domain. Thus Eqs. (55) and (56) may be used to analyze our data.

B. Experimental setup

The experimental setup is shown in Fig. 3. The light pulses ($\lambda_1=556$ nm, $\lambda_2=680$ nm) are delivered by two dye lasers (pulse duration 5 ns, spectral width 3 GHz) which are pumped by the same nitrogen laser. Two White cells,[33] consisting of a large mirror M_1 and two small mirrors M_2 and M_2' with the same $R=60$ cm curvature radius, are used as delay lines. A set of beam splitters permits us to separate and to recombine the direct and delayed laser beams. The three laser pulses copropagate in the interaction cell, Glan prisms are used to polarize the beams, and the polarization of the first two pulses can be rotated by means of a $\lambda/2$ plate operating at $\lambda=556$ nm.

As the vapor cell, we use a stainless-steel tube (diameter 40 mm). Two copper screens, located in the heated part of the tube, confine the vapor within a 40-cm-long volume. The light beams make their way through 2-mm-diam holes which are opened in the screens. The same apertures make the interaction volume communicate with the foreign-gas tank. This device guarantees working in a quasi-thermodynamical-equilibrium regime. The oven temperature is fixed at $\theta=300$ °C; this corresponds to an Yb vapor pressure of 3×10^{-7} torr.

As the laser beams and photon echo are copropagating, we have to use an electro-optical shutter (Pockels cell) which blocks laser light and opens at the time the echo is expected to appear. We use a double-stage shutter, made each of a Pockels cell (Lasermetrics 1070) between crossed Glan-prism polarizers, to get a contrast ratio of 10^6 at least. The high-voltage electric pulse is delivered to the Pockels cell at the proper time by means of an avalanche transistor device triggered by the electronically delayed signal from a photodiode. The rise time of the shutter is less than 10 ns. For long delays (long values of t_3-t_1) and very weak signals, an additional Pockels cell (Gsanger LM7) is inserted to decrease the "tail" of the red laser pulse. Furthermore, a colored filter is used to eliminate the very large two-pulse-echo signal at 556 nm produced by the first two pulses. In a general way, considerable attention is paid to the elimination of any parasitic light. Each measurement is made with and without the first laser pulse and the corresponding signal is subtracted.

A 14-stage fast photomultiplier (La Radiotechnique

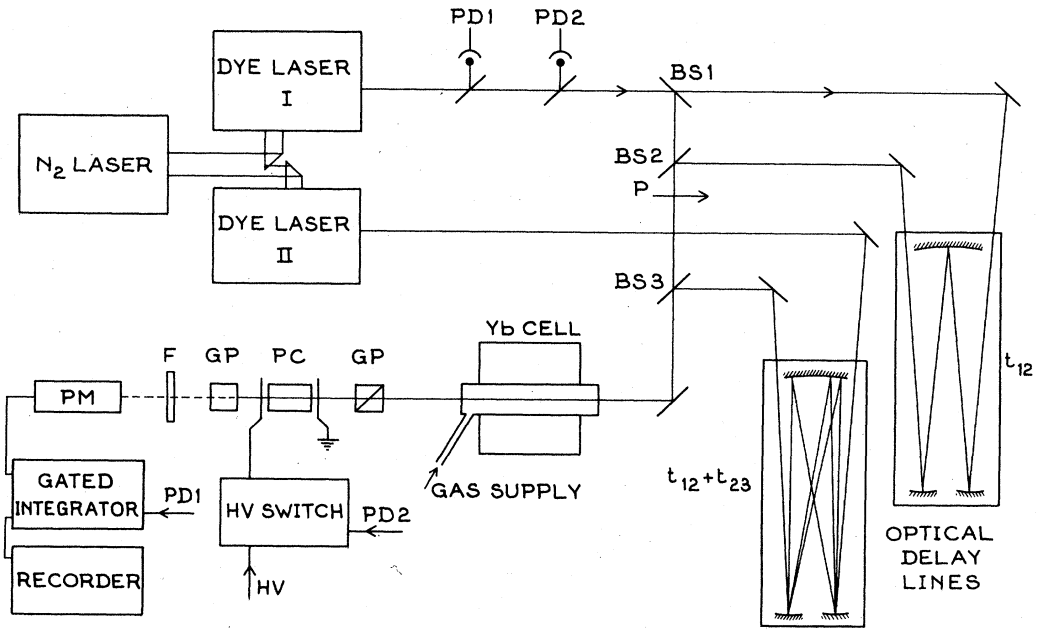

FIG. 3. Experimental setup. PD, photodiode; F, red filter; GP, Glan polarizer; PC, Pockels cell; BS, beam splitter; PM, photomultiplier; P, polarizer.

2254 B) is used to detect the echo and the corresponding output signal is sent to a gated integrator (Princeton Applied Research 162 + 165). For $t_{12}=13.6$ ns the signal amplitude is up to 1 V (50-Ω load) with a neutral-density filter (10^2 attenuation) placed in front of the photomultiplier. Such a high level of signal enables us to increase t_{12} up to 77.6 ns.

We have used a natural mixture of ytterbium but, owing to isotope shifts and hyperfine splittings,[34] we can excite only the zero-nuclear-spin isotopes ($M=172$, 174, and 176) at the center of the line. With μ-metal shielding of the oven for elimination of the earth's magnetic field), the parallel-polarization signal at zero perturber pressure is typically 2000 times smaller than the corresponding crossed-polarization signal.

The measurement procedure is as follows.

(a) First, we set $t_{23}=0$ and we measure the quantity $I_\perp(p)/I_\perp(0)$ for different values of the perturber (noble-gas) pressure. From Eq. (56) we obtain

$$\left[\frac{I_\perp(p)}{I_\perp(0)}\right]^{1/2}=\exp(-\beta_1 p t_{12}) ,$$
$$\beta_1=\frac{d}{dp}\left[\gamma_{ab}+\frac{\omega_1}{\omega_2}\gamma_{bc}\right] . \tag{57}$$

We found, respectively (in units of 10^6 $s^{-1}Torr^{-1}$), $\beta_1^{He}=110$, $\beta_1^{Ne}=51$, $\beta_1^{Xe}=90$.

(b) Then, we set $t_{23}\neq 0$ (typically $t_{23}\approx 60$–90 ns) and we measure the quantity

$$\left[\frac{I_{||}(p)}{I_\perp(p)}\right]^{1/2}=\frac{2-2\exp(-\beta_2 p t_{23})}{2+\exp(-\beta_2 p t_{23})} \tag{58}$$

from which we deduce $\beta_2(t_{12})=d[\Gamma_b^{(2)}(t_{12})-\Gamma_b^{(0)}(t_{12})]/dp$ for different values of t_{12}. The results are discussed in Sec. IV.

(c) Finally, we measure $I_\perp(p)/I_\perp(0$ for $t_{23}\neq 0$ and we obtain $\beta_3(t_{12})=(d/dp)[\Gamma_b^{(0)}(t_{12})]$ from

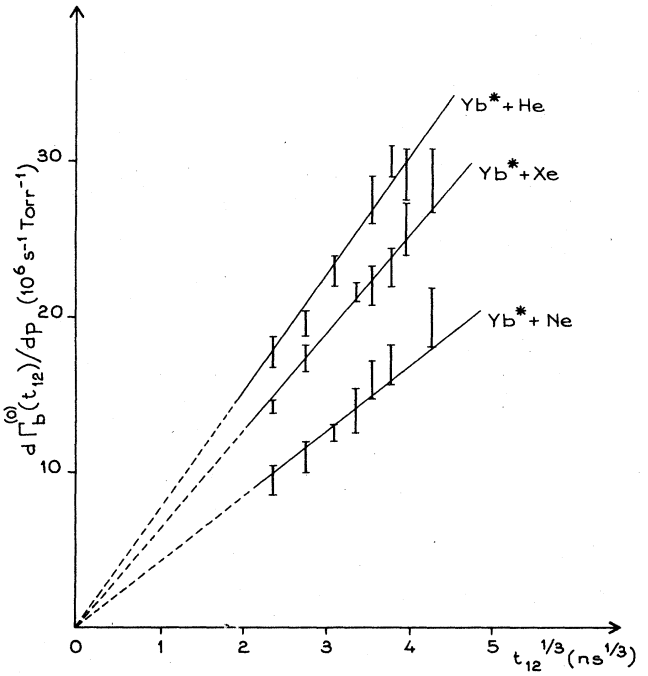

FIG. 4. Elastic collisions between Yb($6s6p\ ^3P_1$) and noble gases. Vertical bars represent experimental data. Fitted calculated rates for elastic scattering are represented by a straight line issuing from the origin.

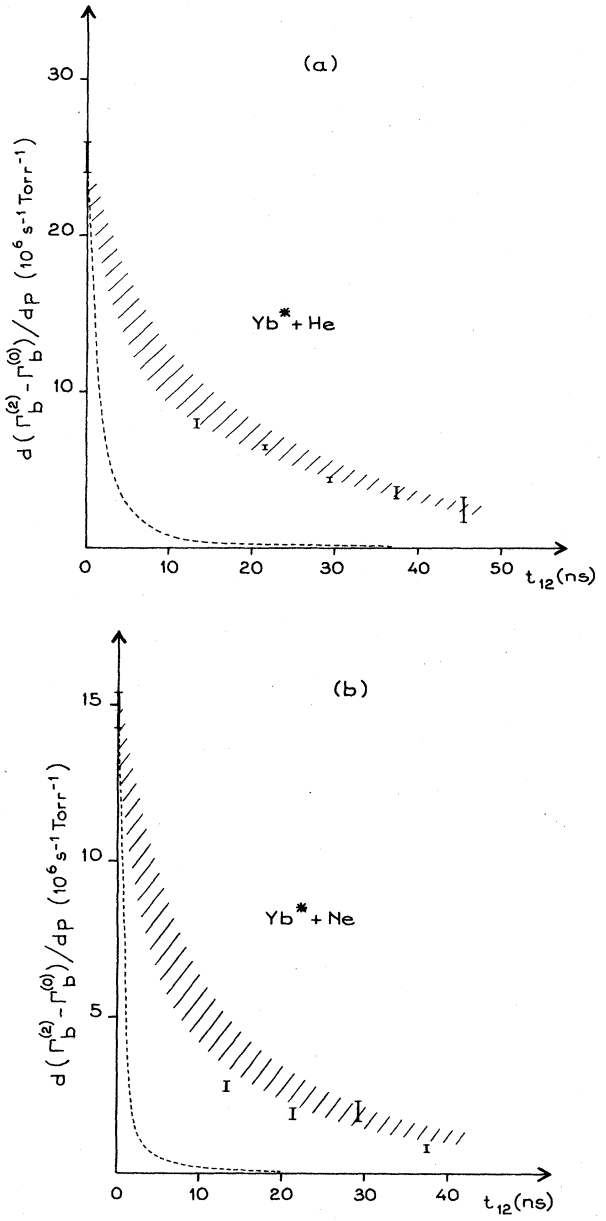

FIG. 5. Collisional depolarization of Yb($6s\,6p\ ^3P_1$) by noble gases. Vertical bars represent experimental data. Dashed lines correspond to hard-sphere model. The hatching results from calculation with the two-component long-range interaction model proposed in the text.

$$\left[\frac{I_\perp(p)}{I_\perp(0)}\right]^{1/2}=\tfrac{2}{3}\exp(-\beta_1 p t_{12})\exp(-\beta_3 p t_{23})\times[1+\tfrac{1}{2}\exp(-\beta_2 p t_{23})]\ . \tag{59}$$

We have neglected the term $\exp(-\gamma_{\text{inel}}t_{23})$ owing to the fact that the $^3P_1$ level is isolated.

Using this measurement procedure, we have obtained $\beta_2(t_{12})$ and $\beta_3(t_{12})$ for values of t_{12} ranging from 13.6 up to 77.6 ns, i.e., for 40 m/s$\geqq\delta v_z\geqq$7 m/s. The experimental results, to be discussed in Sec. IV, are illustrated in Figs. 4 and 5.

IV. RESULTS AND DISCUSSION

A. Elastic scattering in Yb($6s\,6p\ ^3P_1$)—noble-gas collisions

Inversion of the Fourier transform in Eq. (47) should provide us with an "experimental" collision kernel. This operation requires the knowledge of γ^{el}, which is the limit of $\Gamma_b^{(0)}(t_{12})$ as t_{12} tends to infinity. Unfortunately, this limit is out of reach of our experiment since the SPE signal decay, due to phase-interrupting collisions, prevents us from getting data with large enough t_{12} values. Thus we are led to analyze our data through another method. We calculate $\Gamma_b^{(0)}(t_{12})$ in the frame of a simple interaction-potential assumption. Then we adjust the potential parameter through comparison between experimental and calculated $\Gamma_b^{(0)}(t_{12})$ values.

The one-dimensional kernel $W^{(0)}(v_Z',v_Z)$ can be calculated from the elastic scattering differential cross section $d\sigma_{\text{el}}/d\Omega$ by an average over initial perturber velocity and initial active-atom transverse velocity and by a sum over final perturber velocity and final active-atom transverse velocity. According to Eq. (55), $\Gamma_b^{(0)}(t_{12})$ may be expressed in terms of $W^{(0)}(v_Z',v_Z)$:

$$\Gamma_b^{(0)}(t_{12})=\int_{-\infty}^{+\infty}W^{(0)}(0,v_z')dv_z'-\int_{-\infty}^{+\infty}W^{(0)}(0,\zeta_z)\cos(k_1 t_{12}\zeta_z)d\zeta_z\ . \tag{60}$$

As discussed in Ref. 32, and in opposition to previous SPE experiments (Ref. 19), diffractive scattering does not contribute to $\Gamma_b^{(0)}(t_{12})$ in our case. Besides, since the modulation period is much smaller than the mean relative velocity, only small-angle scattering contributes to the restitution terms in $\Gamma_b^{(0)}(t_{12})$. Then, for a long-range C_s/r^s potential, a simple expression is available for the differential cross section $d\sigma_{\text{el}}/d\Omega$ (Appendix A) and we finally obtain[35] (Appendix B)

$$\Gamma_b^{(0)}(t_{12})=N\sigma_{\text{el}}(\bar{u},\theta_{12})\bar{v}_r A(0)\ , \tag{61}$$

where $\bar{u}$ and $\bar{v}_r$ are, respectively, the most probable and the mean relative velocities ($\bar{v}_r=2\bar{u}/\sqrt{\pi}$) and where, according to Eq. (A3),

$$\sigma_{\text{el}}(\bar{u},\theta_{12})=\int_{\theta_{12}}^{\pi}\frac{d\sigma_{\text{el}}}{d\theta}d\theta\ , \tag{62}$$

where $\theta_{12}=(k_1\bar{u}t_{12}\mu/m)^{-1}$ and $A(0)$ is a t_{12}-independent coefficient which is close to unity (Table I). This expression indicates that $\Gamma_b^{(0)}(t_{12})$ may be regarded as the rate of collisions which occurs at a scattering angle larger than θ_{12}. This lower boundary is the scattering angle in the center-of-mass frame, for a collision where the active-atom velocity change is $|\mathbf{v}-\mathbf{v}'|=(k_1 t_{12})^{-1}$. According to Eqs. (A5)—(A11), the t_{12} dependence of $\sigma_{\text{el}}(\bar{u},\theta_{12})$ and of $\Gamma_b^{(0)}(t_{12})$ is $t_{12}^{1/3}$ in a van der Waals potential. This simple $t_{12}^{1/3}$ dependence applies neither at large t_{12}, where diffractive collisions should be considered, nor at small t_{12}, where the small-angle approximation fails. Since $\sigma_{\text{el}}(\bar{u},\theta_{12})$ may be expressed in terms of σ_{el} as a parameter

TABLE I. Experimental and calculated cross sections for elastic scattering of total population and for alignment destruction in Yb*—noble-gas collisions.

	α_B (a_0^3)	$A(0)$	σ_{el} (expt.) (Å^2)	σ_{el} (calc.) (Å^2)	$\sigma^{(2)}$ (expt.) (Å^2)	$\sigma^{(2)}$ (calc.) (Å^2)
He	1.4	0.82	220(20)	173	94(3)	3
Ne	2.7	0.75	320(20)	310	123(7)	6
Xe	27.8	0.73	1240(60)	1034	300(20)	20

(Appendix A), values of σ_{el} are obtained by fitting the calculated expression to the experimental points (Fig. 4). Results are summarized in Table I.

B. Depolarization in Yb($6s\,6p\ ^3P_1$)—noble-gas collisions

We have measured the quantity $d[\Gamma_b^{(2)}(t_{12})-\Gamma_b^{(0)}(t_{12})]/dp$, where, according to Eq. (55)

$$\Gamma_b^{(2)}(t_{12})-\Gamma_b^{(0)}(t_{12})=\int_{-\infty}^{+\infty}[W^{(0)}(0,\zeta_z)-W^{(2)}(0,\zeta_z)]\times\cos(k_1\zeta_z t_{12})/d\zeta_z\ . \quad (63)$$

This is the difference between the restitution terms to population and to alignment. By analogy with the preceding discussion on elastic scattering, this quantity may be regarded as the rate of collisions which, occurring at angles smaller than θ_{12}, destroys atomic alignment. Attention must be paid to the very simple way in which the signal ratio measurements enable us, through determination of $\Gamma_b^{(2)}(t_{12})-\Gamma_b^{(0)}(t_{12})$, to subtract the elastic scattering velocity-changing effect and to isolate the depolarizing-collision-specific velocity-changing effect. Difficulties in performing this subtraction probably caused the previous experimental failure[7,8,11] to observe velocity changes associated with depolarizing collisions.

Our SPE measurements are limited to a few points in the small θ_{12} region. These data need to be complemented by the determination of the total rate for alignment destruction,

$$\gamma_b^{(2)}=\int_{-\infty}^{+\infty}d\zeta_z[W^{(0)}(0,\zeta_z)-W^{(2)}(0,\zeta_z)]\ , \quad (64)$$

which equals the $t_{12}=0$ limit of the quantity $\Gamma_b^{(2)}(t_{12})-\Gamma_b^{(0)}(t_{12})$ which is measured in SPE experiments. The quantity $\gamma_b^{(2)}-[\Gamma_b^{(2)}(t_{12})-\Gamma_b^{(0)}(t_{12})]$ may be regarded as the rate of the collisions which destroy alignment while occurring at a scattering angle larger than θ_{12}. An auxiliary standard photon-echo experiment provides us with $\gamma_b^{(2)}$ (Fig. 6).

A first linearly polarized laser pulse, which is resonant with the a-b transition, populates the sublevel $m=0$ in level b at time $t=0$. Two subsequent laser pulses, in resonance with the b-c transition, irradiate the sample at times T and $T+\tau$. They produce a regular photon echo at time $T+2\tau$ from the population which survives in level b at time T. According to whether their polarization is crossed with or parallel to the first pulse polarization, the last two pulses probe either the $m=0$ or the $m=\pm1$ sublevels. In the latter case the signal is zero in the absence of collisional transfer between Zeeman sublevels. Since no velocity selection operates on level-b multipoles, the ratio of echo signals in crossed and parallel configurations is related to $\gamma_b^{(2)}$ by

$$\left[\frac{I_{\parallel}}{I_{\perp}}\right]^{1/2}=\frac{2-2\exp(-\gamma_b^{(2)}T)}{2+\exp(-\gamma_b^{(2)}T)}\ . \quad (65)$$

From the measurement of this ratio for different values of perturber-gas pressure p we deduce $d\gamma_b^{(2)}/dp$. The corresponding total cross sections for alignment destruction are given in Table I.

As in the case of elastic scattering we compare our data with a calculated expression. Our SPE results for depolarizing collisions are restricted to the case of light perturbers. Thus the relative-velocity distribution may be assumed isotropic (Sec. II B 1). In addition, we assume the following.

(i) A common trajectory for different M sublevels (Sec. II B 3).

(ii) A single trajectory at scattering angle θ (Sec. II B 4). This enables us to express $W^{(2)}(0,\zeta_z)$ in terms of the elastic scattering cross section and of the alignment-decay probability $P^{(2)}(Kb,u)$. In a $j=1$ level, the multipole expansion of the interaction potential is composed of two terms only:

$$V(\mathbf{r},\mathbf{j})=V^{(0)}(r)+\left[j_r^2-\frac{J^2}{3}\right]V^{(2)}(r)\ , \quad (66)$$

where $V^{(0)}(r)$ and $V^{(2)}(r)$ are, respectively, the isotropic

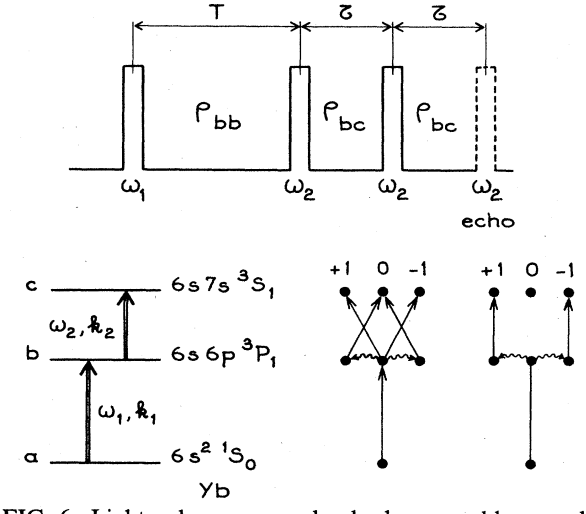

FIG. 6. Light pulse sequence, level scheme, and beam polarizations for measurement of total disalignment rates. Wavy arrows represent collisional transfer between Zeeman sublevels.

and the anisotropic components, and j_r is the j component along the internuclear axis. Long-range interaction is expected to play a dominant role in these large rate collisions. The following potential shapes are thus assumed: (i) $V^{(0)}(r)=-C^{(0)}/r^6$ in the small-angle scattering region and (ii) $V^{(2)}(r)=C^{(2)}/r^6$ in the region where $P^{(2)}(Kb,u)<1$ ($C^{(2)}$ is algebraic).

Within the framework of the common trajectory approximation, the translational motion is fully determined by the isotropic component of the potential. Thus $C^{(0)}$ coincides with the parameter of the elastic scattering potential in level $6s\,6p\,^3P_1$ which has been derived from data in the preceding subsection. The Anderson-model[30] calculation of $\gamma^{(2)}$ leads to

$$\gamma_b^{(2)}=2.5N\bar{v}_r(C^{(2)}/\hbar\bar{u})^{2/5}\ . \tag{67}$$

Comparison with our measurements of $\gamma_b^{(2)}$ enables us to determine $|C^{(2)}|$. Knowing $C^{(0)}$ and $|C^{(2)}|$ we compute $\Gamma_b^{(2)}(t_{1/2})-\Gamma_b^{(0)}(t_{12})$ (Appendix C). Experimental and calculated values of $d[\Gamma_b^{(2)}(t_{12})-\Gamma_b^{(0)}(t_{1/2})]/dp$ are drawn in Fig. 5.

C. Discussion

Both elastic scattering and depolarizing-collision results are compatible with our assumptions on the potential shape. As an illustration of our measurement sensitivity on potential shape we have drawn in Fig. 5 the curve corresponding to hard-core depolarization. It lies well beneath the experimental points. According to the Anderson model, the contribution to $\gamma^{(2)}$ of collisions with $P^{(2)}(Kb,u)<1$ amounts to $0.25\gamma^{(2)}$ in the case of a $1/r^6$ potential [cf. Eqs. (C5) and (C6)]. Small-angle depolarizing collisions that we detect in our SPE experiments contribute at most 20% (Yb-Ne) and 30% (Yb-He) to the alignment total decay rate $\gamma^{(2)}$. Thus these collisions occur precisely in the region where $P^{(2)}(Kb,u)<1$ and where the potential dependence of $P^{(2)}(Kb,u)$ affects the Anderson-model calculation of the depolarizing differential cross section [cf. Eq. (C7)]. The long-range $1/r^6$ behavior of the interatomic potential corresponds to a dipole-dipole interaction. In collisions which involve ground-level rare-gas perturbers, a usual approximation identifies the energy denominator in a dipole-dipole pseudopotential with the rare-gas ionization energy. Then the dipole-dipole pseudopotential between an active atom A and a perturber B is

$$V(\mathbf{r},\mathbf{j})=-\frac{1}{r^6}\alpha_B(\langle\Psi|\mathbf{P}_A^2|\Psi\rangle+\tfrac{1}{2}\langle\Psi|3(P_{Az})^2-\mathbf{P}_A^2|\Psi\rangle), \tag{68}$$

where α_B is the perturber polarizability and $\mathbf{P}_A$ is the active-atom dipole-moment operator. For an ns-$n'p$ state one obtains[36]

$$V^{(0)}(r)=\alpha_B(\langle r^2\rangle_p+\langle r^2\rangle_s-\tfrac{2}{3}|r_{sp}|^2)\ , \tag{69}$$

$$V^{(2)}(r)=\tfrac{1}{2}\alpha_B(\tfrac{3}{5}\langle r^2\rangle_p-|r_{sp}|^2)\ . \tag{70}$$

Radial integrals may be calculated in a parametric central potential. For Yb($6s\,6p\,^3P_1$) one obtains[37] $\langle r^2\rangle_{6s}=15.54a_0^2$, $\langle r^2\rangle_{6p}=25.30a_0^2$, $\langle r\rangle_{6s\,6p}=-3.89a_0$. Using tabulated values for α (Ref. 38) we calculate $V^{(0)}(r)$, $V^{(2)}(r)$, and the corresponding elastic scattering and depolarization cross sections (Table I). A reasonable agreement is obtained for elastic scattering. On the contrary, calculated anisotropy is much smaller than indicated by our measured depolarization cross sections. This suggests that short-range interaction may dominate the depolarizing process. Thus our initial assumption of $1/r^6$-potential behavior is questioned.

In a $^3P_1$ level the potential anisotropy may be analyzed in terms of two potential curves,

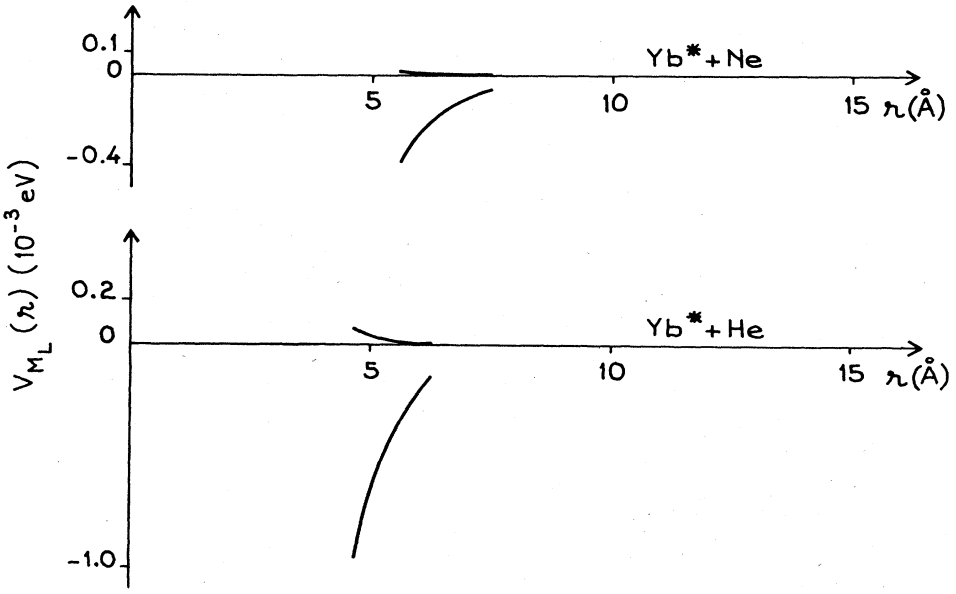

FIG. 7. Potential curves from data analysis with the two-component long-range interaction model. Upper curves and lower curves represent $V_{M_L=0}(r)$ and $V_{M_L=1}(r)$ components, respectively.

$$V_{M_L=0}(r)=V^{(0)}(r)+\tfrac{4}{3}V^{(2)}(r)\ , \tag{71}$$

$$V_{M_L=\pm1}(r)=V^{(0)}(r)-\tfrac{2}{3}V^{(2)}(r)\ , \tag{72}$$

which express the potential dependence on the electronic orbital momentum component M_L along the internuclear axis. In the dipole-dipole interaction region our previous calculation indicates that $V_{M_L=0}\sim V_{M_L=1}$. Potential curves depart from the each other at shorter distances due to short-range interaction anisotropy. Since the short-range interaction is generally more repulsive in $M_L=0$ than in $M_L=1$ we may suppose that $V_{M_L=0}$ lies above $V_{M_L=1}$. Thus $V^{(2)}(r)>0$. Knowledge of the sign of $V^{(2)}(r)$ enables us to determine $V_{M_L=0}(r)$ and $V_{M_L=1}(r)$ from our previous determination of $V^{(0)}(r)$ and of $V^{(2)}(r)$. Corresponding curves are represented in Fig. 7. It appears that $V_{M_L=0}(r)$ is very close to zero in the explored angular domain. Thus, in this region

$$V^{(2)}(r)\simeq-\tfrac{1}{2}V_{M_L=1}(r)\ . \tag{73}$$

Consistency between our initial assumption of a $1/r^6$ potential shape and the existence of a short-range interaction is preserved provided we assume that $V_{M_L=0}(r)$ alone is affected by short-range forces and that $V_{M_L=1}(r)$ remains close to a van der Waals potential in our region of interest.

V. CONCLUSION

We have demonstrated that SPE techniques can be used to realize angular analysis of collisional scattering. Comparison between experiment and calculation has been performed, starting with a long-range r^{-6} model potential. For the first time in a nonlinear laser spectroscopy experiment, velocity changes which accompany depolarizing collisions have been measured. This has been made possible by the very simple way in which the SPE signal ratio subtracts the velocity-changing effect corresponding to elastic scattering from that which is specific to depolarizing collisions. Stimulated-photon-echo techniques should be extended to investigation of other quasiresonant processes such as transfers between fine-structure levels and rovibrational levels or as energy-pooling collisions. Processes which slightly change atomic translational motion, such as electronic collisions, might also be examined.

Working with a gas sample imposes some drastic limitations on the SPE method. In particular, velocity averaging washes out fine details such as rainbow oscillations and orbiting resonances. However, the coarse information which is displayed in a SPE experiment may be valuable. Active atoms are detected inside the collision volume so that both ground-state and short-lived excited atoms may be monitored. The magnitudes of the cross section are determined, not only their variations. Both elastic and inelastic processes may be considered.

Finally, storing a modulation inside the velocity distribution of active atoms may be regarded as a way of marking them. It should be possible to follow this modulation through reactive processes in order to identify reaction paths.

ACKNOWLEDGMENT

Laboratoire Aimé Cotton is "Laboratoire associé à l'Université Paris—Sud."

APPENDIX A: CLASSICAL ELASTIC SCATTERING IN A LONG-RANGE r^{-s} POTENTIAL

1. Small-angle-deflection function

The relation between the scattering angle θ and the impact parameter b in the small-deflection domain, as given by classical mechanics for a $-C/r^s$ potential, is[24]

$$\theta=(s-1)Cf(s)/Eb^s\ , \tag{A1}$$

where

$$f(s)=\sqrt{\pi}\,\Gamma\left[\frac{s}{2}-\frac{1}{2}\right]\Big/2\Gamma(s/2)\ . \tag{A2}$$

$E=\frac{1}{2}\mu u^2$ (μ=reduced mass, u=relative velocity) is the kinetic energy available for the collision.

2. Integral expression of the scattering cross section

The contribution to the total scattering cross section of collisions with an impact parameter $b<b_0$ is πb_0^2. If the short-range contribution to the small-angle scattering may be neglected and if b_0 lies in the long-range interaction region, one may thus write

$$\pi b_0^2\simeq\int_{\Omega_0}\frac{d\sigma_{\rm el}}{d\Omega}d\Omega=\sigma_{\rm el}(u,\theta_0)\ . \tag{A3}$$

The integration domain Ω_0 refers to collisions with a scattering angle $\theta>\theta_0(b_0)$, where $\theta_0(b_0)$ is the scattering angle for an impact parameter b_0. For large b_0 and small θ_0, Eq. (A1) can be used for $b(\theta)$ and Eq. (A3) gives

$$\sigma_{\rm el}(u,\theta_0)=\pi s g(s)(C/E\theta_0)^{2/s}\ , \tag{A4}$$

where

$$g(s)=[(s-1)f(s)]^{2/s}/s\ . \tag{A5}$$

3. Small-angle differential cross section for elastic scattering

The small-angle differential cross section can be obtained from

$$\frac{d\sigma_{\rm el}}{d\Omega}=2\pi b\left|\frac{db}{d\Omega}\right|=b\left|\frac{db}{\sin\theta\,d\theta}\right|\ . \tag{A6}$$

Substitution of (A2) in (A6) gives

$$\frac{d\sigma_{\rm el}}{d\Omega}=g(s)(C/E\theta)^{2/s}/\theta\sin\theta \tag{A7}$$

or as $\theta\ll1$

$$\frac{d\sigma_{\rm el}}{d\Omega}=g(s)(C/E\theta)^{2/s}\theta^{-2}\ . \tag{A8}$$

4. Semiclassical total elastic cross section

The semiclassical approximation leads to the following expression for the *total* elastic cross section (including diffractive collision contribution) in a $-C/r^s$ potential:[24]

$$\sigma_{\rm el}=p(s)\left[\frac{C}{\hbar u}\right]^{2/(s-1)}+\text{glory contribution}\ , \tag{A9}$$

where

$$p(s)=\pi^2[2f(s)]^{2/(s-1)}/\sin[\pi/(s-1)]\Gamma[2/(s-1)]\ .$$

Neglecting the glory contribution to $\sigma_{\rm el}$, the classical scattering cross section $\sigma_{\rm el}(u,\theta_0)$ and $d\sigma_{\rm el}/d\Omega$ can be expressed using $\sigma_{\rm el}$ instead of C as a parameter:

$$\frac{d\sigma_{\rm el}}{d\Omega}=\frac{1}{s}(s-1)^{2/s}\times\left[\frac{1}{\pi^2}\sin\left[\frac{\pi}{s-1}\right]\Gamma\left[\frac{2}{s-1}\right]\right]^{(s-1)/s}\times\theta^{-2}\sigma_{\rm el}(K^2\sigma_{\rm el}\theta^2)^{-1/s}\ , \tag{A10}$$

$$\sigma_{\rm el}(u,\theta)=\pi s\left[\frac{d\sigma_{\rm el}}{d\Omega}\right]\theta^2\ , \tag{A11}$$

where $K=\mu u/\hbar$.

APPENDIX B: ELASTIC SCATTERING DECAY RATE

We intend to determine

$$\gamma(t_{12},v_z)=\int W_{00}^{00}(v_z,v_z')dv_z'-\int W_{00}^{00}(v_z,v_z+\zeta_z)\times\cos(k\zeta_z t_{12})d\zeta_z\ , \tag{B1}$$

where $W_{00}^{00}(v_z,v_z')$ is given by Eq. (38). The following assumptions are used.

(i) $k\bar{u}t_{12}(\mu/m)\gg 1$. This means that only small-angle scattering contributes to the restitution term.

(ii) $k\Delta v_z^d t_{12}\ll 1$ where $\Delta v_z^d=2\sqrt{\pi}\hbar/m\sqrt{\sigma_{\rm el}}$. This means that diffractive collisions do not perturb the modulation stored in the velocity distribution, so that they do not contribute to $\gamma(t_{12},v_z)$. Their contributions to the departure term and the restitution term balance each other.

(iii) Small-angle scattering is mainly due to the long-range interaction potential which varies as r^{-s}.

According to Eqs. (15) and (43),

$$W_{00}^{00}(v_z',v_z)=N\int d^3u\,d^3u'dv_\perp dv_\perp'\delta(\mathbf{v}'-\mathbf{v}-\mathbf{Y})\times W_p(\mathbf{v}_p')W(\mathbf{v}_\perp')\delta(u-u')\times u^{-1}(d\sigma_{\rm el}/d\Omega)\ , \tag{B2}$$

where

$$d\sigma_{\rm el}/d\Omega=\frac{1}{2j+1}\sum_{M,M'}|f_{MM'}^{\rm hel}(u,R'')|^2\ . \tag{B3}$$

Reduction of the ten-dimensional integral to a three-dimensional (3D) integral leads to [39]

$$W_{00}^{00}(v_z',v_z)=N\left[\frac{m}{\mu}\right]^2\frac{2}{(\pi)^{1/2}\bar{u}}\int_{-\infty}^{+\infty}\int_{-\infty}^{+\infty}dX\,dY\,e^{-X^2-Y^2}\int_1^\infty dZ\,e^{-p^2(Z)}\frac{d\sigma_{\rm el}}{d\Omega}\frac{|\zeta_Z|}{(1+\beta^2)^{1/2}}\ , \tag{B4}$$

where

$$p^2(Z)=\left[\left[\frac{m}{2\mu}Z\right]^2\frac{\zeta_z^2}{1+\beta^2}+\frac{1+\beta^2}{Z^2}\left[v_z'-\frac{\zeta_z}{2}\right]^2-\frac{m}{\mu}\left[v_z'-\frac{\zeta_z}{2}\right]\zeta_z\right]\Big/\bar{u}^2\ , \tag{B5}$$

$$\frac{u^2}{\bar{u}^2}=X^2+\left[1+\frac{\beta^2}{Z^2}\right]\left[\frac{Y}{(1+\beta^2)^{1/2}}+\left[\frac{v_z'}{\bar{u}}-\frac{\zeta_z}{2\bar{u}}\right]\left[1-\frac{1}{Z^2}\right]^{1/2}\right]^2+\left[\frac{m}{2\mu}\right]^2\frac{\zeta^2}{\bar{u}^2}\ , \tag{B6}$$

$$\zeta=|\mathbf{v}'-\mathbf{v}|=\frac{\mu}{m}|\mathbf{u}'-\mathbf{u}|=|\zeta_z|\left[\frac{Z^2+\beta^2}{1+\beta^2}\right]^{1/2}\ , \tag{B7}$$

$$\zeta_z=v_z'-v_z\ . \tag{B8}$$

When $d\sigma_{\rm el}/d\Omega$ falls off rapidly as θ increases and when $(m/\mu)\zeta_z\ll\bar{u}$, $P^2(Z)$ and $u^2/\bar{u}^2$ reduce to

$$P^2(Z)\simeq(1+\beta^2)(v_z')^2/\bar{u}^2Z^2\ , \tag{B9}$$

$$\frac{u^2}{\bar{u}^2}\simeq X^2+\left[1+\frac{\beta^2}{Z^2}\right]\left[\frac{Y}{(1+\beta^2)^{1/2}}+\frac{v_z'}{\bar{u}}\left[1-\frac{1}{Z^2}\right]^{1/2}\right]^2\ . \tag{B10}$$

Let us define an angle θ_c which fulfills the following two conditions:

$$\theta_c>\theta_d=\Delta v_z^d/u\ , \tag{B11}$$

$$\theta_c<\theta_{12}=(k\bar{u}t_{12}\mu/m)^{-1}\ . \tag{B12}$$

The former condition indicates that θ_c lies in the classical scattering region and the latter condition implies that collisions at $\theta<\theta_c$ do not contribute to $\gamma(t_{12},v_z)$. Compati-

bility of these two requirements is guaranteed by assumption (ii). Thus, in the calculation of $\gamma(t_{12},v_z)$ we may replace the differential cross section $d\sigma_{\rm el}/d\Omega$ by

$$\frac{d\sigma'_{\rm el}}{d\Omega}=\begin{cases} d\sigma_{\rm el}/d\Omega & \text{if } \theta>\theta_c \\ 0 & \text{if } \theta<\theta_c \end{cases} . \tag{B13}$$

The cutoff angle θ_c is chosen so that $\theta_c=\bar{\theta}_c\bar{u}/u$. Thus,

$$\frac{d\sigma'_{\rm el}}{d\Omega}=\frac{d\sigma_{\rm el}}{d\Omega}H\left[\frac{\zeta}{\bar{u}\,\bar{\theta}_c}\right] , \tag{B14}$$

where

$$H(x)=0 \quad \text{if } x<1 ,$$
$$H(x)=1 \quad \text{if } x\geq 1 . \tag{B15}$$

Let us denote $W_{00}^{00'}(v'_z,v_z)$ and $\gamma'(t_{12},v_z)$ as the collision kernel and the modulation decay rate which are calculated using $d\sigma'_{\rm el}/d\Omega$ instead of $d\sigma_{\rm el}/d\Omega$. It results from the previous discussion that within the limits of our initial assumptions [Eqs. (B11) and (B12)]

$$\gamma'(t_{12},v_z)=\gamma(t_{12},v_z) . \tag{B16}$$

The restitution term in $\gamma'(t_{12},v_z)$ may be written as

$$\begin{aligned}\int W_{00}^{00'}(v_z,v_z+\zeta_z)&\cos(k_1\zeta_z t_{12})d\zeta_z \\ &=\int W_{00}^{00}(v_z,v_z+\zeta_z)[\cos(k_1\zeta_z t_{12})-1]d\zeta_z \\ &\quad+\int W_{00}^{00'}(v_z,v_z+\zeta_z)d\zeta_z ,\end{aligned} \tag{B17}$$

where $W_{00}^{00}(v_z,v'_z)$ has been substituted for $W_{00}^{00'}(v_z,v'_z)$ in the first term on the right-hand side as a consequence of the definition of θ_c. Substitution of Eqs. (A7) and (B14) in (B17) leads to

$$\begin{aligned}\int W_{00}^{00'}(v_z,v_z+\zeta_z)&\cos(k_1\zeta_z t_{12})d\zeta_z \\ &=N\sigma_{\rm el}(\bar{u},\theta_{12})\bar{v}_r A(v_z)+N\sigma_{\rm el}(\bar{u},\bar{\theta}_c)\bar{v}_r B(v_z) ,\end{aligned} \tag{B18}$$

where

$$A(v_z)=(2/\pi s)\Gamma(-2/s)\cos\pi/s \times\int_1^{+\infty} dZ\,F(Z,v_z/\bar{u}) , \tag{B19}$$

$$B(v_z)=(2/\pi s)\int_0^{+\infty} X^{-1-2/s}dX \times\int_1^{+\infty} dZ\,F(Z,v_z/\bar{u}) \times H\left[X\left[\frac{Z^2+\beta^2}{1+\beta^2}\right]^{1/2}\right] , \tag{B20}$$

$$\begin{aligned}F\left[Z,\frac{v_z}{\bar{u}}\right]&=(1+\beta^2)^{-1/2}\left[\frac{Z^2+\beta^2}{1+\beta^2}\right]^{-1-1/s} \\ &\quad\times\exp[-(\beta^2v_z^2/Z^2\bar{v}^2)] \\ &\quad\times\int_{-\infty}^{+\infty}\int_{-\infty}^{+\infty} dX\,dY(u/\bar{u})^{2-2/s} \\ &\quad\times\exp[-(X^2+Y^2)] ,\end{aligned} \tag{B21}$$

and $\sigma_{\rm el}(u,\theta)$ is defined by Eq. (A4). Then we use Eq. (A3) in order to put the departure term in $\gamma'(t_{12},v_z)$ into the form

$$\begin{aligned}\int W'(v_z,v'_z)dv'_z &=(N/\pi^{3/2})\frac{1}{\bar{v}_p\bar{u}^2} \\ &\quad\times\int d^3u\,\sigma_{\rm el}(u,\theta_c)u \\ &\quad\times\exp\{-[(u_\perp^2/\bar{u}^2)+(u_z-v_z)^2/\bar{v}_p^2]\}\end{aligned} \tag{B22}$$

$$=N\sigma_{\rm el}(\bar{u},\bar{\theta}_c)\bar{v}_r C(v_z) , \tag{B23}$$

where

$$C(v_z)=\frac{1}{2\bar{v}_p^2\bar{u}^2}\int d^3u\,(u/\bar{u})^{1-2/s} \times\exp\{-[(u_\perp^2/\bar{u}^2)+(u_z-v_z)^2/\bar{v}_p^2]\} . \tag{B24}$$

Combining departure and restitution terms we obtain

$$\begin{aligned}\gamma'(v_z,t_{12})&=N\sigma_{\rm el}(\bar{u},\theta_{12})\bar{v}_r A(v_z) \\ &\quad+N\sigma_{\rm el}(\bar{u},\theta_c)\bar{v}_r[B(v_z)-C(v_z)] .\end{aligned} \tag{B25}$$

According to Eq. (B16), this expression does not depend upon $\bar{\theta}_c$. Thus

$$B(v_z)=C(v_z) . \tag{B26}$$

The final result is

$$\gamma(t_{12},v_z)=N\sigma_{\rm el}(\bar{u},\theta_{12})\bar{v}_r A(v_z) . \tag{B27}$$

According to Eq. (45), the relaxation rate of the modulation stored in the velocity distribution of a level's total population is given by

$$\Gamma^{(0)}(t_{12})=\int W_L(v_z)\gamma(t_{12},v_z)dv_z . \tag{B28}$$

The v_z dependence of $\gamma(t_{12},v_z)$ is mainly located in the factor $\exp[-(\beta^2v_z^2/Z^2\bar{v}^2)]$ which appears in Eq. (B21). Thus, when $\beta^2\ll 1$, this factor is close to unity and

$$\Gamma^{(0)}(t_{12})\simeq\gamma(t_{12},0) . \tag{B29}$$

Another limiting case occurs when the coherent spectral width of the laser pulses is much larger than the Doppler width. Then, $W_L(v_z)\simeq W(v_z)$ and integration over v_z leads to

$$\Gamma^{(0)}(t_{12})\simeq\gamma(t_{12},0)\beta/[(1+\beta^2)^{1/2}\arctan\beta] . \tag{B30}$$

APPENDIX C: ANDERSON-MODEL CALCULATION

The aim of this appendix is to achieve a simple-model calculation of

$$\begin{aligned}\Gamma^k(t_{12})-\Gamma^{(0)}(t_{12}) &=\int_{-\infty}^{+\infty} d\zeta_z\cos(k\zeta_z t_{12}) \\ &\quad\times[W^{(0)}(0,\zeta_z)-W^k(0,\zeta_z)]d\zeta_z .\end{aligned} \tag{C1}$$

The quantity $W^{(0)}(0,\zeta)-W^k(0,\zeta)$ is expressed in Eq. (39)

in terms of the elastic scattering differential cross section and of the k-multipole decay probability, assuming isotropic relative-velocity distribution, common trajectory for different M sublevels, and single trajectory at scattering angle θ (cf. Secs. II B 1, II B 3, and II B 4). Under the approximation that the transverse motion is separated from the longitudinal one, Eq. (39) may be substituted into Eq. (43). By integrating over $\mathbf{v}_\perp$ and $\mathbf{v}'_\perp$ one obtains

$$W^k(0,\zeta_z)-W^{(0)}(0,\zeta_z)=N\int d^3Y\,d^3u\,\delta(\zeta_z-Y_z)W_r(\mathbf{u}')\times\delta(u-u')u^{-1}\frac{d\sigma^{(0)}}{d\Omega}P^k(J_\theta,u)\ , \tag{C2}$$

where $\zeta=|\boldsymbol{\zeta}|$. Remember that the requirement $m_p\ll m$ is implied in the initial assumption of isotropic relative-velocity distribution. Then, reduction of Eq. (C2) to a 3D integral leads to

$$W^k(0,\zeta_z)-W^{(0)}(0,\zeta_z)\simeq\frac{2}{\sqrt{\pi}}\left[\frac{m}{\mu}\right]^2\frac{N}{\bar{u}}\int_{-\infty}^{+\infty}\int_{-\infty}^{+\infty}e^{-X^2-Y^2}dX\,dY\int_{|\zeta_z|}^{\infty}\frac{d\sigma^{(0)}}{d\Omega}P^k(J_\theta,u)\exp\left[-\left[\frac{m}{2\mu}\frac{\zeta}{\bar{u}}\right]^2\right]d\zeta\ , \tag{C3}$$

where

$$\frac{u^2}{\bar{u}^2}=X^2+Y^2+\left[\frac{m}{2\mu}\right]^2\frac{\zeta^2}{\bar{u}^2}\ .$$

Then, setting $w=k\zeta t_{12}$, $\xi=k\zeta_z t_{12}$, and $\theta_{12}=k\bar{u}t_{12}\mu/m$, and integrating by parts, we obtain

$$\Gamma^k(t_{12})-\Gamma^{(0)}(t_{12})=2N\bar{v}_r\theta_{12}^2\int_0^\infty d\xi\sin\xi\int_{-\infty}^{+\infty}\int_{-\infty}^{+\infty}dX\,dY\,e^{-X^2-Y^2}\frac{d\sigma^{(0)}}{d\Omega}P^k(J_\theta,u)\exp[-(\xi\theta_{12}/2)^2]\ . \tag{C4}$$

The variation of $P^k(J,u)$ as a function of the impact parameter $b=J/K$ in a long-range $1/r^s$ potential has been studied extensively.[5] As the impact parameter decreases, $P^k(J,u)$ increases continuously up to about unity. Then, as b keeps decreasing, $P^k(J,u)$ oscillates. The Anderson model[30] consists in doing the following.

(i) Replacing $P^k(J,u)$ by an asymptotic expression $P^k_{\rm as}(J,u)$ for $b>b_k$, where b_k is such that $P^k_{\rm as}(Kb_k,\mu)=1$. Actually, the validity range of $P^k_{\rm as}(Kb_k,u)$ should be restricted to the region where $P^k(J,u)\ll 1$, i.e., $|V_M(r)-V_{M'}(r)|\ll\hbar u/b$.

(ii) Setting $P^k(J,u)=1$ for $b>b_k$. This means that oscillations are replaced by a mean value which is assumed equal to unity.

In summary, the Anderson model leads to

$$P^k(J,u)=\begin{cases}(b_k/b)^{2/(s-1)} & \text{for } b>b_k\\ 1 & \text{for } b<b_k\ .\end{cases} \tag{C5}$$

As a consequence, the k-multipole-destruction cross section is

$$\Sigma^k=\int_0^\infty P^k(Kb,u)2\pi b\,db=\pi b_k^2(s-1)/(s-2)\ . \tag{C6}$$

In the long-range small-angle scattering region the impact parameter b and the scattering angle θ are connected by Eq. (A2). Since a common trajectory has been assumed for different M sublevels, the elastic scattering potential may be identified with either component $V_M(r)$. Equivalently, it may be identified with the isotropic component $V^{(0)}(r)=\sum_M V_M(r)/(2j+1)$. Conversely, the elastic scattering potential constant can be expressed in terms of Σ^k and of θ_k which is the scattering angle at b_k. Finally, we obtain

$$\frac{d\sigma^{(0)}}{d\Omega}P^k(J,u)=\begin{cases}\dfrac{1}{\pi s}\left[\dfrac{s-2}{s-1}\right]\Sigma^k\left[\dfrac{\theta_k}{\theta}\right]^{-1+4/s}\theta_k^{-2} & \text{for } \theta<\theta_k\\ \dfrac{1}{\pi s}\left[\dfrac{s-2}{s-1}\right]\Sigma^k\left[\dfrac{\theta_k}{\theta}\right]^{2/s+1}\theta_k^{-2} & \text{for } \theta>\theta_k\ .\end{cases} \tag{C7}$$

The impact parameter b_k is connected with the potential anisotropy through the equation

$$P^k_{\rm as}(Kb_k,u)=1\ , \tag{C8}$$

where, for $j=1$,[36]

$$P^k_{\rm as}(Kb,u)=g_k\left[\frac{b}{\hbar u}I_{s-2}\frac{\sqrt{2}}{\sqrt{3}}[V^{(2)}(b)]^2\right]^2\times\left[1-\frac{3}{s}+\frac{3}{s^2}\right], \tag{C9}$$

where

$$I_s=2\times\frac{2}{3}\times\cdots\times\frac{s-1}{s},\ s\text{ odd}\qquad I_s=\frac{\pi}{2}\times\frac{3}{4}\times\cdots\times\frac{s-1}{s},\ s\text{ even} \tag{C10}$$

and where $g_1=\frac{1}{2}$ and $g_2=\frac{3}{10}$. Then we substitute $m\zeta/\mu u$ for θ in Eq. (C7) and transport this latter expression into (C4). We perform integration over ξ in the limit of experimental interest $\theta_{12}\ll 1$. We obtain

$$\Gamma^k(t_{12})-\Gamma^{(0)}(t_{12})=\frac{2}{s}N\bar{v}_r\left[\frac{s-2}{s-1}\right]\bar{\Sigma}^k\int_0^{+\infty}dr\,e^{-r}\left\{r^{1-1/s}\left[r^{-1/s(s-1)}\left[\frac{\sin y}{y}+\frac{s}{2}\cos y\right]-\frac{s}{2}x^{2/s}\mathrm{Re}[e^{i\pi/s}\Gamma(1-2/s,iy)]\right]\left[1+\frac{2}{s}\right]^{-1}+r^{1-2/s}x^{-2+4/s}\mathrm{Re}[e^{2i\pi/s}\gamma(1-4/s,iy)]\right\}, \tag{C11}$$

where $x=\bar{\theta}_k/\theta_{12}$, $y=xr^{1/2(s-1)}$, $\bar{\Sigma}^k=\Sigma^k(\bar{u})$, $\bar{\theta}_k=\theta_k(\bar{u})$; $\Gamma(\alpha,x)$ and $\gamma(\alpha,x)$ are Euler's incomplete gamma functions. An approximate expression is obtained by setting $x\simeq y$. Then,

$$\Gamma^k(t_{12})-\Gamma^{(0)}(t_{12})\simeq\frac{2}{s}N\bar{v}_r\left[\frac{s-2}{s-1}\right]\bar{\Sigma}^k\left[\Gamma\left[2-\frac{1}{s-1}\right]\left[\frac{\sin x}{x}+\frac{s}{2}\cos x-\frac{s}{2}x^{2/s}\mathrm{Re}[e^{i\pi/s}\Gamma(1-2/s,ix)]\right]\left[1+\frac{2}{s}\right]^{-1}+\Gamma\left[2-\frac{2}{s}\right]x^{-2+4/s}\mathrm{Re}[e^{2i\pi/s}\gamma(1-4/s,ix)]\right]. \tag{C12}$$

A limiting case of experimental interest occurs when depolarizing collisions do not preserve the modulation in velocity space at a scattering angle larger than θ_k. Then, $x\gg1$ and Eq. (C12) reduces to

$$\Gamma^k(t_{12})-\Gamma^{(0)}(t_{12})=\frac{2}{s}N\bar{v}_r\left[\frac{s-2}{s-1}\right]\bar{\Sigma}^k\Gamma\left[2-\frac{2}{s}\right]\cos\left[\frac{2\pi}{s}\right]\Gamma\left[1-\frac{4}{s}\right]x^{-2+4/s}. \tag{C13}$$

This expression exhibits a $t_{12}^{-2+4/s}$ dependence. An expression similar to (B27) may be found in this limiting case:

$$\Gamma^k(t_{12})-\Gamma^{(0)}(t_{12})=N\bar{v}_r[\sigma^{(0)}(u,\theta_{12})-\sigma^k(u,\theta_{12})]2\cos\frac{2\pi}{s}\left[\frac{s-2}{s-4}\right]\Gamma\left[2-\frac{2}{s}\right]\Gamma\left[2-\frac{4}{s}\right], \tag{C14}$$

where

$$\sigma^k(u,\theta_{12})=\int_{\theta_{12}}^{\pi}\frac{d\sigma^k}{d\theta}d\theta\,. \tag{C15}$$

The $t_{12}=0$ limit of $\Gamma^k(b_{12})-\Gamma^{(0)}(b_{12})$ cannot be obtained from the small-angle expression (C11). It may be derived from Eqs. (36) and (C6). One obtains

$$\gamma^k=\Gamma^k(0)-\Gamma^{(0)}(0)=N\int d^3u\,W_r(\mathbf{u})u\Sigma^k=N\bar{v}_r\Gamma\left[2-\frac{1}{s-1}\right]\bar{\Sigma}^k. \tag{C16}$$

[1]K. Bergman, U. Hefter, and J. Witt, J. Chem. Phys. **72**, 4777 (1980).

[2]Ch. Bender, W. Beyer, H. Haberland, D. Hausamann, and H. P. Ludescher, J. Phys. (Paris) Colloq. **46**, C1-75 (1985).

[3]W. D. Phillips, J. A. Serri, D. J. Ely, D. E. Pritchard, K. R. Way, and J. L. Kinsey, Phys. Rev. Lett. **41**, 937 (1978).

[4]W. J. Alford, K. Burnett, and J. Cooper, Phys. Rev. A **27**, 1310 (1983); W. J. Alford, N. Andersen, K. Burnett, and J. Cooper, *ibid.* **30**, 2366 (1984).

[5]E. L. Lewis, Phys. Rep. **58**, 1 (1980), and references therein.

[6]W. Happer, Rev. Mod. Phys. **44**, 169 (1972).

[7]T. W. Hansch and P. Toschek, IEEE J. Quantum Electron. **QE-5**, 61 (1969); R. Keil, A. Schabert, and P. Toschek, Z. Phys. **261**, 71 (1973).

[8]I. Colomb and M. Dumont, Opt. Commun. **21**, 143 (1977); I. Colomb, M. Gorlicki, and M. Dumont, *ibid.* **21**, 289 (1977).

[9]J. E. Thomas, A. P. Ghosh, C. D. Nabors, M. Attili, A. Forber, and M. S. Feld, in Technical Digest of the XIII International Quantum Electronics Conference, Anaheim, California, 1984 (unpublished), p. 68.

[10]S. N. Atutov, S. G. Rautian, G. D. Rodionov, E. G. Saprykin, and A. M. Shalagin, Opt. Spektrosk. **49**, 1041 (1980) [Opt. Spectrosc. (USSR) **49**, 569 (1980)].

[11]J. L. Le Gouët and R. Vetter, J. Phys. B **13**, L147 (1980).

[12]R. L. Shoemaker, S. Stenholm, and R. G. Brewer, Phys. Rev. A **10**, 2037 (1974).

[13]S. M. Freund, J. W. C. Johns, A. R. W. Mac Kellar, and T. Oka, J. Chem. Phys. **59**, 3445 (1973).

[14]T. W. Meyer and C. K. Rhodes, Phys. Rev. Lett. **32**, 637 (1974); W. K. Bischel and C. K. Rhodes, Phys. Rev. A **14**, 176 (1976).

[15]T. W. Mossberg, R. Kachru, S. R. Hartmann, and A. M. Flusberg, Phys. Rev. A **20**, 1976 (1979).

[16]R. Kachru, T. J. Chen, S. R. Hartmann, T. W. Mossberg, and P. R. Berman, Phys. Rev. Lett. **47**, 902 (1981).

[17]T. W. Mossberg, R. Kachru, and S. R. Hartmann, Phys. Rev. Lett. **44**, 73 (1980).

[18]R. A. Forber, L. Spinelli, J. E. Thomas, and M. S. Feld, Phys. Rev. Lett. **50**, 331 (1983).

[19]T. W. Mossberg, A. Flusberg, R. Kachru, and S. R. Hartmann, Phys. Rev. Lett. **42**, 1665 (1979); R. Kachru, T. W. Mossberg, and S. R. Hartmann, Opt. Commun. **30**, 57 (1979).

[20]M. Fujita, H. Nakatsuka, H. Nakanischi, and M. Matsuoka, Phys. Rev. Lett. **42**, 974 (1979).

[21]J. C. Keller and J. L. Le Gouët, Phys. Rev. Lett. **52**, 2034 (1984).

[22]J. L. Le Gouët and P. R. Berman, Phys. Rev. A **24**, 1831 (1981); **25**, 34 (1982).
[23]M. Jacob and G. C. Wick, Ann. Phys. (N.Y.) **7**, 404 (1959).
[24]M. S. Child, *Molecular Collision Theory* (Academic, London, 1974).
[25]J. B. Delos, W. R. Thorson, and S. K. Knudson, Phys. Rev. A **6**, 709 (1972); **6**, 720 (1972).
[26]A. R. Edmonds, *Angular Momentum in Quantum Mechanics* (Princeton University, Princeton, N.J., 1960).
[27]M. Abramowitz and I. A. Stegun, *Handbook of Mathematical Functions* (Dover, New York, 1970).
[28]P. J. Brussaard and H. A. Toloek, Physica (Utrecht) **23**, 955 (1957).
[29]P. R. Berman, Phys. Rev. A **5**, 927 (1972); **6**, 2157 (1972).
[30]A. Omont, J. Phys. (Paris) **26**, 26 (1964); Prog. Quantum Electron. **5**, 69 (1977).
[31]A. S. Dickinson and D. Richards, Adv. At. Mol. Phys. **18**, 165 (1982).
[32]J. L. Le Gouët and J. C. Keller, in *Proceedings of the Seventh International Conference on Spectral Line Shapes,* edited by F. Rostas (De Gruyter, Berlin, 1985).
[33]J. U. White, J. Opt. Soc. Am. **32**, 285 (1942).
[34]D. L. Clark, M. E. Cage, D. A. Lewis, and G. W. Greenless, Phys. Rev. A **20**, 239 (1979).
[35]$\Gamma_b^{(0)}(t_{12})$ is the quantity which is named $\gamma_b^{\rm el}(t_{12})$ in Ref. 21. In this paper an incorrect determination of $\int W(\Delta v_z)d\Delta v_z$ leads to an erroneous expression for $\gamma_b^{\rm el}(t_{12})$. Indeed, the small scattering angle limit for $W(\Delta v_z)$ is improperly used in this integral which is the departure term. Appendix B presents the proper derivation of this quantity.
[36]J. P. Faroux, Thèse d'Etat, Université de Paris, 1969.
[37]M. Aymar (private communication).
[38]A. Dalgarno and A. E. Kingston, Proc. R. Soc. London, Ser. A **259**, 424 (1960).
[39]A. P. Kol'chenko, S. G. Rautian, and A. M. Shalagin, Nuclear Physics and Semiconductor Physics Institute of the Siberian Division of the Soviet Academy of Science Internal Report, 1972 (unpublished).